1968

Electronic properties and magnetic ordering of light rare-earth metals

Gerald Stephen Fleming
Iowa State University

69-9856

FLEMING, Gerald Stephen, 1940-
ELECTRONIC PROPERTIES AND MAGNETIC ORDERING OF LIGHT RARE-EARTH METALS.

Iowa State University, Ph.D., 1968
Physics, solid state

University Microfilms, Inc., Ann Arbor, Michigan

ELECTRONIC PROPERTIES AND MAGNETIC ORDERING OF LIGHT RARE-EARTH METALS

by

Gerald Stephen Fleming

A Dissertation Submitted to the
Graduate Faculty in Partial Fulfillment of
The Requirements for the Degree of
DOCTOR OF PHILOSOPHY

Major Subjects: Physics

Approved:

Signature was redacted for privacy.

In Charge of Major Work

Signature was redacted for privacy.

Head of Major Department

Signature was redacted for privacy.

Dean of Graduate College

Iowa State University
Of Science and Technology
Ames, Iowa

1968

TABLE OF CONTENTS

I INTRODUCTION

The rare-earth metals have been the subject of much interest in recent years because of their interesting magnetic properties. With the exceptions of lanthanum, lutecium and ytterbium these metals have partially filled 4f electron shells resulting in a highly localized magnetic moment given by Hund's rules. These metals exist in a paramagnetic state until the temperature is reduced below some critical value at which the moments become arranged in an ordered structure.

The crystal structures of the rare-earth metals and their magnetic moment arrangements have been determined by neutron diffraction and other experimental methods (Koehler 1965). These measurements have shown that the heavy rare earths from gadolinium through lutecium have a simple hexagonal close-packed crystal structure with the exception of Yb which crystallizes in a face-centered cubic structure.

The last two rare earths Yb and Lu have completely filled 4f electron shells and only exhibit weak paramagnetic properties. The remaining heavy rare-earth metals all exist in one or more ordered magnetic states at low temperatures. Gadolinium transforms directly from the paramagnetic state to a ferromagnetic state at about room temperature while terbium and dysprosium become ferromagnetic at low enough temperature after going through an antiferromagnetic phase. The remaining heavy metals in the series holmium, erbium and thulium transform from the paramagnetic state to a periodic moment arrangement and then at lower temperatures transform into helical ferromagnetic or antidomain structures.

In all of these ordered states the moments within a given hexagonal

layer are parallel but their orientation varies from one layer to the next. In Tb, Dy and the helical phase of Ho the moments all lie in the basal plane. In the other structures the moments also have a component along the c-axis of the crystal.

The light rare-earth metals are considerably more complex both in crystal structure and moment arrangement. The first two elements in the series lanthanum and cerium occur in both face-centered cubic and double hexagonal close-packed crystal structures. Ce is found in both of these states at room temperature but at lower temperatures it transforms into a more densely packed fcc phase. In lanthanum both phases exist together with the dhcp structure being more common. Praseodymium and neodymium, the next two metals in the series, also occur in this double hexagonal close-packed structure. After promethium, which has no stable isotope, comes samarium which has the most complex structure of any of the rare-earth metals. The Sm crystal structure is basically hexagonal but it goes through nine layers before it repeats itself. Sm appears to be antiferromagnetic but its magnetic structure has not been determined.

The last of the light rare-earths is europium which occurs in a body-centered cubic structure. It transforms from a paramagnetic state to an antiferromagnetic state at 91K. It is unique among the rare-earths having ordered phases in that its paramagnetic moment indicates that Eu is divalent while all the other metals discussed are trivalent.

The magnetic properties of the dhcp rare-earths are considerably different from those of the other rare-earths. La has no localized moment and thus no ordered magnetic state. The ordering in Ce is difficult to determine because of the existence of three phases in the crystal structure

and the dependence of the structure on the preparation of the sample. However, it appears that an antiferromagnetic transition occurs at 12.5K with the moments arranged parallel to the c-axis.

For Nd and Pr there are ordered moment arrangements observed at low temperatures where the periodicity of the ordering is in the basal plane rather than along the c-axis. In Nd the existing neutron diffraction data may be explained by a model for which the moments at the sites with hcp nearest neighbors order at 18K with a periodicity described by a wavevector equal to $.13\underline{b}_1$, where $\underline{b}_1$ is a reciprocal lattice basis vector in the hexagonal plane (Moon, et al., 1964). From this temperature down to 7.5K the moments at sites with fcc symmetry are randomly orientated. At 7.5K these moments also become ordered with a periodicity having a propagation vector parallel to that for the first ordering and with a magnitude of $.15\underline{b}_1$. Although the two propagation vectors are parallel and of nearly equal magnitude the moments at the hcp sites lie along a $\underline{b}$ direction while those in the fcc sites are in an $\underline{a}$ direction of the crystal.

The ordering for Pr occurs at 25K and appears to be identical to the first ordering in Nd. The modulation vector for this ordering is $.13\underline{b}_1$, as for Nd but there is no second ordering down to 1.4K (Cable, et al., 1964).

The mechanism which produces ordering of localized moments in the rare-earths is indirect exchange. This occurs when the conduction electrons in the vicinity of a localized moment are polarized by direct exchange with that moment. The resulting conduction electron polarization acts to align neighboring moments. Ruderman and Kittel (1954) showed that the energy of a system of localized moments was lowered by this indirect exchange between the moments.

This energy perturbation can also be expressed as the energy of the conduction electrons in an effective magnetic field produced by the localized magnetic moments. The ratio of the conduction electron magnetization characterized by wave vector $\underline{q}$ to the effective field component with the same periodicity defines the generalized susceptibility $\chi(q)$.

The generalized susceptibility is proportional to the Fourier transform of the indirect exchange constant. The wave vector for which this latter quantity is maximized was shown by Villain (1959) to correspond to the periodicity of the magnetic ordering in the metal. Lomer (1962) observed that for chromium this wave vector of the magnetic ordering was equal to the separation of two large flat regions of the Fermi surface of that metal. Roth, et al., (1966) showed that the largest Fourier components of the indirect exchange constant occurred for wave vectors equal to the spacing between Fermi surface pieces with low curvature.

Calculations which have been made on the heavy rare-earth metals show that the Fermi surface can be used to predict the occurrence of magnetic ordering. The band structures and Fermi surfaces of these metals were determined by Dimmock and Freeman (1964) and by Keeton and Loucks (1968) who noted the presence of large regions of the surface which were perpendicular to the c-axis. These pieces of surface occurred for all of the metals except Gd and were separated by a wave vector approximately equal to the periodicity of the periodic moment arrangement. They stressed that the absence of these regions in Gd was responsible for that element being ferromagnetic rather than antiferromagnetic. These observations were verified analytically by Evenson and Liu (1968a) who computed the generalized susceptibilities of several of these heavy rare-earths. Their

results showed that there was a maximum in $\chi(q)$ near the value expected from the observed ordering in the antiferromagnetic metals and that there was no such maximum value for Gd.

It is the purpose of this investigation to study the relationship of the Fermi surfaces of the light rare-earth metals to the observed electronic properties and magnetic configurations. The energy bands which are used to determine the Fermi surface are calculated using the relativistic augmented plane-wave method (Loucks, 1965). This technique is a relativistic reformulation of the augmented-plane-wave method originally proposed by Slater (1937) and has been successfully used to calculate the band structures of the heavy rare-earths (Keeton and Loucks 1968). It is based on the assumption that the Hartree-Fock one electron potential can be approximated by a spherically symmetric potential within a sphere centered about each atom and by a constant potential in the region between the spheres. This "muffin-tin" potential admits exact solutions to the Dirac equation in each of these two regions. Matching the wave functions at the surface of the spheres and using the variational method to find the best combination of solutions one can find the energy eigenvalues of the conduction electrons.

The density of states at the Fermi energy is calculated for each metal using the bands previously determined. The values calculated are consistently 20 to 30 percent below the numbers determined experimentally from specific heat measurements. If a correction is included to account for electron-phonon interaction then a density of states is obtained which is due only to the band structure. Applying this correction to the experimental results gives values comparable to those which are calculated here.

The Fermi surfaces for the light rare-earth metals differ principally

from those of the heavier metals of the series in that there are no large flat regions perpendicular to the c-axis. The perturbation to the potential of a simple hcp lattice introduced by the dhcp structure appears to be responsible for the elimination of these pieces of Fermi surface.

The absence of these flat regions eliminates the nesting which is responsible for the ordering of the heavy rare-earths. The most noticeable nesting for Nd and Pr is between Fermi surface pieces perpendicular to one of the b axes of the reciprocal lattice. This observation is confirmed by the generalized susceptibility calculations which indicate that the magnetic ordering periodicity should be in the b direction.

This susceptibility peak gives a b axis periodicity which agrees with the model given by Koehler (1965) but indicates that the moments in the four layers of the dhcp cell should be aligned parallel to each other. There is a second peak in the generalized susceptibility curve which would produce an ordering with alternate layers antiferromagnetically aligned but the wave vector for the periodicity in the basal plane is considerably smaller than that which has been observed.

This latter peak is broader and flatter than the first one and the location of its maximum value is affected greatly by the wave vector dependence of the indirect exchange matrix element. The peak at .125b is much sharper and relatively unaffected by the choice of matrix element. It appears that it is this peak which is responsible for the magnetic ordering and that the observed ordering between adjacent hexagonal layers may be due to some additional interaction.

II CRYSTAL STRUCTURE AND POTENTIAL

A. Structure of the Light Rare-Earth Elements

While the heavy rare-earth elements with unfilled 4f shells all crystallize in a simple hexagonal close-packed structure, the light rare-earth elements have much more complex crystal structures (Gschneidner, 1961). The observed crystal structures for the light rare-earth elements (La-Sm) are listed in Table 1.

The crystal structure which will be of concern here is the double hexagonal close-packed structure. Both neodynium and praseodymium have a dhcp structure while lanthanum and cerium have a face-centered cubic phase as well as a dhcp phase. The lattice constants, a and c, for the dhcp phases are also given in Table 1. (Pearson, 1958).

The double hexagonal close-packed crystal is formed by stacking close-packed hexagonal layers in the sequence ABACABAC... where the layer orientation can be visualized by comparison to the hexagonal close-packed structure (ABAB...) and the cubic close-packed structure (ABCABC...). A drawing of this structure is shown in Figure 1. It can be seen that the atoms in the B and C layers have the same nearest neighbors as does an atom in an hcp crystal. The atoms in the A layers have the same nearest neighbors as does an atom in an fcc lattice. Thus there are two inequivalent sites in the lattice which makes the dhcp lattice unique among the rare-earth crystal structures.

The unit cell for the dhcp lattice consists of four atoms located at (0,0,0), (1/3, 2/3, 1/4), (0,0,1/2) and (2/3, 1/3, 3/4) where (p,q,r) means $p\underline{a}_1 + q\underline{a}_2 + r\underline{a}_3$ where the $\underline{a}_i$ are the basic translation vectors of

Table 1. Properties of light rare-earth metals

Element	Z	Crystal Structure	DHCP Lattice Constants (a.u.)
La	57	dhcp, fcc	7.1244, 22.9775
Ce	58	dhcp, fcc (two phases)	-
Pr	59	dhcp	6.9401, 22.3659
Nd	60	dhcp	6.9125, 22.2975
Pm	61	(unstable)	-
Sm	62	9 layer hexagonal	-

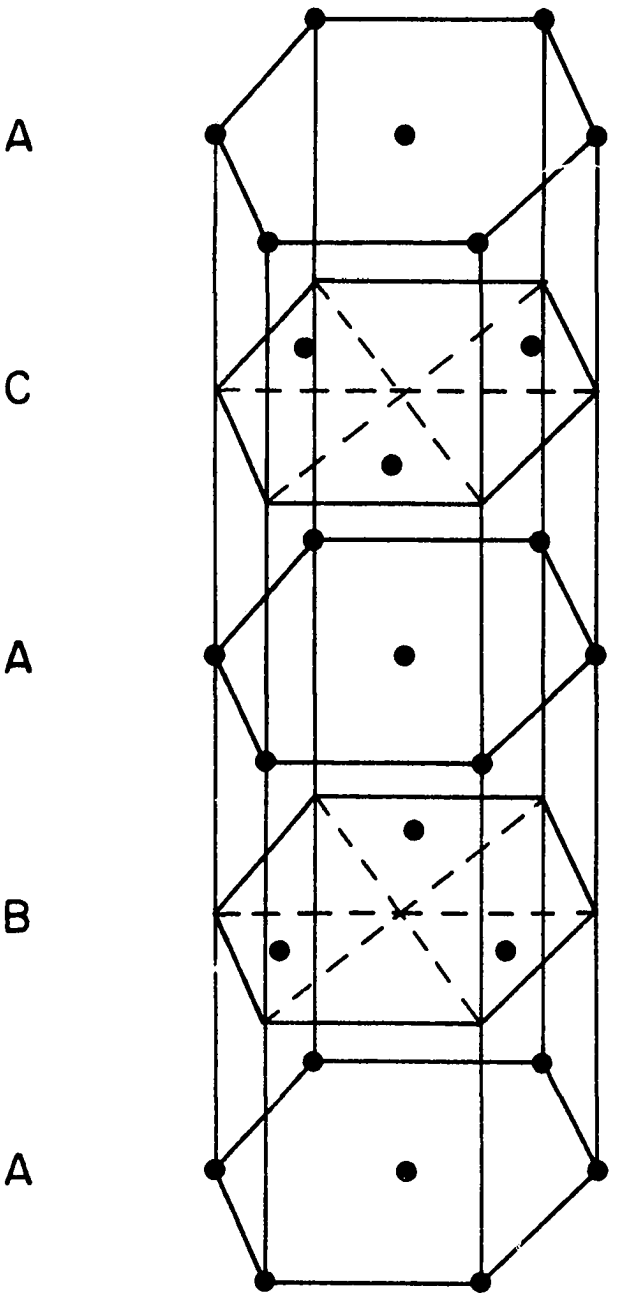

Figure 1. Double hexagonal close-packed crystal structure

the lattice. In terms of the lattice constants c and a given by Pearson (1958) these vectors can be written

$$\underline{a}_1 = a\hat{i}$$

$$\underline{a}_2 = -\frac{1}{2} a\hat{i} + \sqrt{\frac{3}{2}}\, a\hat{j}$$

$$\underline{a}_3 = c\hat{k} \qquad (1)$$

where $\hat{i}$, $\hat{j}$ and $\hat{k}$ are a set of orthonormal basis vectors. These lattice vectors are such that the potential, which is periodic throughout the crystal, has the property that

$$V(\underline{r} + \underline{\tau}) = V(\underline{r}) \qquad (2)$$

where $\underline{\tau} = n_1\underline{a}_1 + n_2\underline{a}_2 + n_3\underline{a}_3$ for any integers n_1, n_2, n_3.

B. Potential in a DHCP Lattice

In order to calculate the electron states for a crystal it is necessary to approximate the real potential by some potential for which the Dirac equation can be solved exactly. The model which has been proved most satisfactory is the muffin-tin potential (Ziman, 1965). In this model the potential is spherically symmetric within a radius R_ν (which is less than half the nearest neighbor distance) about each atomic site and is constant in the region outside these spheres.

The crystal potential which is used to construct the muffin-tin potential consists of coulombic and exchange potentials which are calculated separately using the method proposed by Mattheiss (1964). The coulombic potential consists of contributions from the nuclear charge and from the electronic distribution and can be expressed as

$$V_o(r) = 2Z/r - U_o(r) \tag{3}$$

where Z is the nuclear charge and U_o is the solution to Poisson's equation

$$\nabla^2 U_o(r) = -8\pi\rho_o(r). \tag{4}$$

The electronic charge density for an atom, $\rho_o(r)$, has been calculated in a relativistically self-consistent manner by Liberman, et al., (1965).

The total coulombic potential consists of contributions from all the atoms in the crystal and at a distance r from an atom can be written

$$V_c(r) = V_o(r) + \sum_i V_o(a_i|r) \tag{5}$$

where the summation is over the neighboring atoms in the crystal. $V_o(a_i|r)$ is the component of the potential due to the atom at a_i which is spherically symmetric about the central atom (Lowdin, 1956).

$$V(a_i|r) = \frac{1}{2a_i r} \int_{a-r}^{a+r} xV(x)d^3x \quad . \tag{6}$$

In these calculations the summation in Equation 5 is made over all atoms within two and one-half times the nearest neighbor distance from a given atom. The terms due to more distant atoms are negligible since the electronic charge density due to atoms at this distance is of the order of 10^{-5} of the nearest neighbor contributions. There are 14 shells within this distance of any atom in the crystal. The radii of these shells and the number of atoms in each shell for the two inequivalent sites in the dhcp lattice are listed in Table 2.

The exchange contribution to the potential was approximated by the Slater (1951) exchange term

Table 2. Distances of nearest neighbor atoms for dhcp lattice

Shell Number	Plane A Number of Atoms	Plane A Distance	Planes B,C Number of Atoms	Planes B,C Distance
1	1	0	1	0
2	6	$\sqrt{\frac{a^2}{3}+\frac{c^2}{16}}$	6	$\sqrt{\frac{a^2}{3}+\frac{c^2}{16}}$
3	6	a	6	a
4	6	$\sqrt{\frac{4a^2}{3}+\frac{c^2}{16}}$	6	$\sqrt{\frac{4a^2}{3}+\frac{c^2}{16}}$
5	2	$\frac{c}{2}$	6	$\sqrt{\frac{a^2}{3}+\frac{c^2}{16}}$
6	12	$\sqrt{\frac{7a^2}{3}+\frac{c^2}{16}}$	12	$\sqrt{\frac{7a^2}{3}+\frac{c^2}{16}}$
7	6	$3a$	6	$3a$
8	12	$\sqrt{a^2+\frac{c^2}{4}}$	6	$\sqrt{\frac{4a^2}{3}+\frac{c^2}{4}}$
9	6	$2a$	6	$2a$
10	12	$\sqrt{\frac{13a^2}{3}+\frac{c^2}{16}}$	12	$\sqrt{\frac{7a^2}{3}+\frac{c^2}{16}}$
11	12	$\sqrt{3a^2+\frac{c^2}{4}}$	12	$\sqrt{\frac{13a^2}{3}+\frac{c^2}{16}}$
12	6	$\sqrt{\frac{16a^2}{3}+\frac{c^2}{16}}$	6	$\sqrt{\frac{16a^2}{3}+\frac{c^2}{16}}$
13	6	$\sqrt{\frac{a^2}{3}+\frac{9c^2}{16}}$	6	$\sqrt{\frac{a^2}{3}+\frac{9c^2}{16}}$
14	12	$\sqrt{4a^2+\frac{c^2}{4}}$	12	$\sqrt{\frac{13a^2}{3}+\frac{c^2}{4}}$

$$V_{ex}(r) = -6\left(\frac{3}{8\pi}\rho(r)\right)^{1/3} \tag{7}$$

where the electronic charge density

$$\rho(r) = \rho_o(r) + \sum_i \rho_o(a_i|r) \tag{8}$$

consists of the contribution, $\rho_o(r)$, due to the electronic charge density of the nearest atom and contributions due to neighboring atoms. In these calculations the summation was again over the atoms listed in Table 2.

The value of the potential which is used (Loucks, 1967) in the region between the APW spheres is the spherical average of the actual potential in the region between the APW sphere and the Wigner-Seitz sphere. The Wigner-Seitz sphere has a radius r_o chosen so that its volume equals one-fourth the volume of the unit cell. This average potential is then given by

$$V_a = 3\int_s^{r_o}[V_c(r) + V_{ex}(r)]r^2dr/(r_o^2-S^2) \tag{9}$$

where S is the APW sphere radius. It is convenient to set the potential in this region to zero and thus the potential inside the muffin-tin spheres can finally be written

$$V(r) = V_c(r) + V_{ex}(r) - V_a \ . \tag{10}$$

Calculation of the potentials for the two lattice sites showed them to be equal to within the accuracy of the computer program (.01 percent). Since the spherically symmetric potential is the same around each atom site, the radial wave function in the vicinity of an hcp nearest neighbor site is the same as in the neighborhood of a site with cubic symmetry. This will greatly reduce the complexity of the RAPW wave functions as will be shown in the next chapter.

III. ENERGY BAND CALCULATIONS

A. The Reciprocal Lattice and Brillouin Zone

Because of the translational symmetry of the crystal potential, the itinerant electron wavefunctions must satisfy the Block theorem

$$\psi_{\underline{k}}(\underline{r} + \underline{\tau}) = e^{i\underline{k}\cdot\underline{\tau}} \psi_{\underline{k}}(\underline{r}), \tag{11}$$

where $\underline{\tau}$ is a basic translation vector if the direct lattice as defined in the preceding section and $\underline{k}$ is the wave vector which defines the state of the electron. It is evident that if

$$\underline{k}' = \underline{k} + \underline{g} \tag{12}$$

where

$$\underline{g} \cdot \underline{\tau} = 2n\pi \tag{13}$$

then this state is also labelled by the wave vector $\underline{k}'$. Such a vector $\underline{g}$ is called a reciprocal lattice vector. Those values of $\underline{k}$ for which no non-zero $\underline{g}$ exists such that $|\underline{k} + \underline{g}| < |\underline{k}|$ are said to lie in the first Brillouin zone of reciprocal space. A state $\underline{k}'$ can now be defined by an equivalent state $\underline{k}$ lying within the Brillouin zone and a certain band index. Thus all N states of the N itinerant electrons in a real crystal will be represented by a wave vector, $\underline{k}$, in the first Brillouin zone and by a band index, n.

B. The APW Method

A technique which has been effectively used to calculate energy bands in metals is the augmented-plane-wave (APW) method. Originally proposed by Slater (1937) the APW method became highly practical with the development

of high speed computers. This method assumes that the crystal potential can be approximated by the muffin-tin potential described previously. In the region between the APW spheres the solution to the Schrödinger equation is a sum of plane wave terms

$$\phi(\underline{k},\underline{r}) = e^{i\underline{k}\cdot\underline{r}} . \tag{14}$$

In the APW sphere the potential is spherically symmetric so the wave functions can be written as

$$\phi(r) = \sum_{\ell=0}^{\infty} \sum_{m=-\ell}^{\ell} A_{\ell m} Y_{\ell m}(\theta,\varphi) R_{\ell}(r) \tag{15}$$

where $Y_{\ell m}$ is a spherical harmonic, R_{ℓ} is the solution of the radial wave equation and the $A_{\ell m}$ are constants to be determined by the boundary conditions.

The boundary conditions are such that the wave function and its derivative must be continuous at the APW sphere. By expanding the plane wave solution in terms of spherical harmonics (Loucks, 1967) the constants $A_{\ell m}$ in Equation 15 can be determined.

A set of these plane wave solutions with wave vectors $\underline{k} + \underline{g}_i$, where $\underline{k}$ is the reduced wave vector and $\underline{g}_i$ is a reciprocal lattice vector can be used as basis functions and the solution to the wave equation for the periodic potential can be written as a variational function

$$\psi(\underline{k},\underline{r}) = \sum_i c_i \phi(\underline{k} + \underline{g}_i, \underline{r}) \tag{16}$$

where the coefficients c_i are determined by minimizing the energy with respect to every coefficient. From the trial function the energy eigenvalues for a given $\underline{k}$ can be determined by solving the secular determinant. Since the dimension of this determinant is equal to the number of recipro-

cal lattice vectors (recips) used in the trial wave function, it is necessary to keep the number of recips as small as possible without sacrificing any accuracy in the determination of the eigenvalues. The set of recips used in the band calculations is determined by first choosing a very large set and calculating the eigenvalues at high symmetry points in the Brillouin zone and then eliminating recips which produce negligible changes in these eigenvalues. The set used at one point in the zone may not produce good convergence at another point so some additional recips may have to be included so that good convergence is obtained throughout the zone.

C. The RAPW Method

It has been shown by Keeton (1966) that for elements as heavy as the lanthanides relativistic effects must be included in the energy band calculations. This is accomplished by using the APW method to solve the Dirac equation with a muffin-tin potential. This theory known as the relativistic augmented-plane-wave (RAPW) method (Loucks, 1965) is used to determine the energy eigenvalues following steps analogous to those used in the APW method.

After matching the wave functions at the APW sphere and minimizing the energy with respect to the coefficients in the variational function it is then necessary to solve the secular determinant given by Loucks (1967, p. 82). Before this can be evaluated the terms involving the structure factor must be simplified. These terms are of the form

$$S_{ij} = C_{ij} \sum_{\nu} S_{\nu}^{2} \, e^{i\underline{g}_{ij} \cdot \underline{r}_{\nu}} \qquad (17)$$

where the sum is over the APW spheres in the unit cell, S_{ν} is the radius of the νth sphere, $\underline{r}_{\nu}$ is the location of the center of the νth sphere, C_{ij} are constants and

$$\underline{g}_{ij} = \underline{g}_j - \underline{g}_i \cdot \tag{18}$$

Since the potentials around each lattice site were found to be identical, the APW spheres were constructed to be of the same size. For the dhcp lattice Equation 17 can be rewritten

$$S_{ij} = C_{ij} S^2 \sum_{\nu=1}^{4} e^{i\underline{g}_{ij} \cdot \underline{r}_\nu} \cdot \tag{19}$$

Inserting the coordinates of the four atoms in the units cell the structure factor reduces to

$$S_{ij} = C_{ij} S^2 [(-1)^{n_1+n_2} + (-1)^{n_1+n_2+n_3} + 2\cos\pi(\frac{n_1}{3} - \frac{n_2}{3} - \frac{n_3}{2})] \tag{20}$$

where the n_k are defined by

$$\underline{g}_{ij} = 2\pi \sum_{k=1}^{3} n_k \underline{b}_k \tag{21}$$

where the basis vectors of the reciprocal lattice are defined by

$$\underline{b}_i = \frac{\underline{a}_j \times \underline{a}_k}{\underline{a}_i \cdot \underline{a}_j \times \underline{a}_k} \tag{22}$$

where i,j,k is a cyclic permutation of 1,2,3. The structure factor can then be inserted in the RAPW matrix element and the secular determinant evaluated to find the energy eigenvalues.

D. Energy Bands for DHCP Lanthanum

Lanthanum is the lightest of the rare earth elements and exists in both fcc and dhcp phases. Its atomic number is 57 and its metallic atomic configuration is $5d^1 6s^2$. Since there are four atoms in the dhcp unit cell and three conduction electrons per atom it has six filled energy bands since each band admits states of both spins. Although there are no 4f electrons

there has been some concern that the 4f levels may have a pronounced effect on the electronic properties. Preliminary calculations indicated that the 4f levels lie well above the Fermi energy and were assumed to have negligible effect on the Fermi surface and thus they were not included in the calculations. From the work of Waber and Switendick (1965) on fcc cerium it was decided that the 4f levels for that element lie very near the Fermi energy and could not be neglected. For that reason cerium has been excluded from these calculations.

The energy eigenvalues for La were calculated along the high symmetry directions of the Brillouin zone shown in Figure 2 using 41 reciprocal lattice vectors. The energy bands along high symmetry directions are shown in Figure 3. The set of recips used is listed in Table 3. These recips gave eigenvalues which were converged to within .002 Rydberg at the high symmetry points in the Brillouin zone. Eigenvalues were then calculated over a mesh of 63 uniformly spaced points in the 1/24th zone and were interpolated to give the energy levels at the 462 mesh points in the 1/24th zone shown in Figures 4 and 5. This is equivalent to calculating eigenvalues at 7200 points in the first zone. The interpolation was performed using spline fits (Pennington, 1965) through the points at which eigenvalues had been previously determined with the boundary condition that at a zone boundary

$$\left.\frac{\partial E}{\partial k}\right|_{\text{normal}} = 0 \ . \tag{23}$$

The density of states for lanthanum from this calculation is shown in Figure 6. The solid curve which has also been plotted is the integrated density of states. From these data the Fermi energy was determined to lie

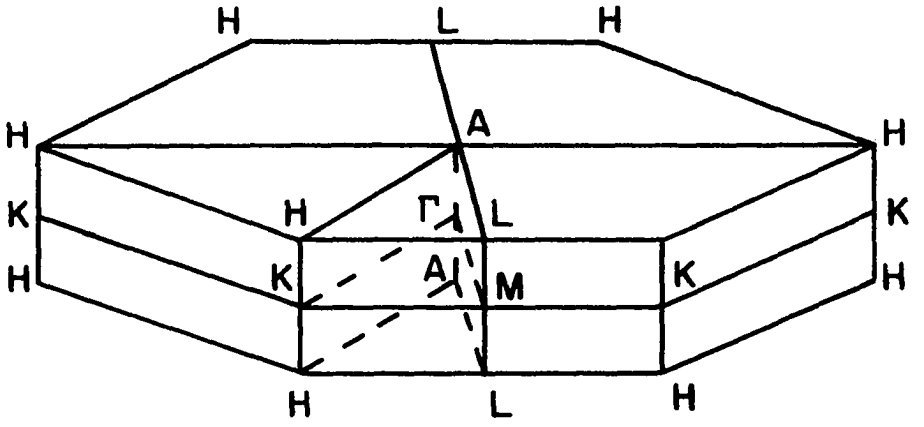

Figure 2. Brillouin zone for double hexagonal close-packed lattice

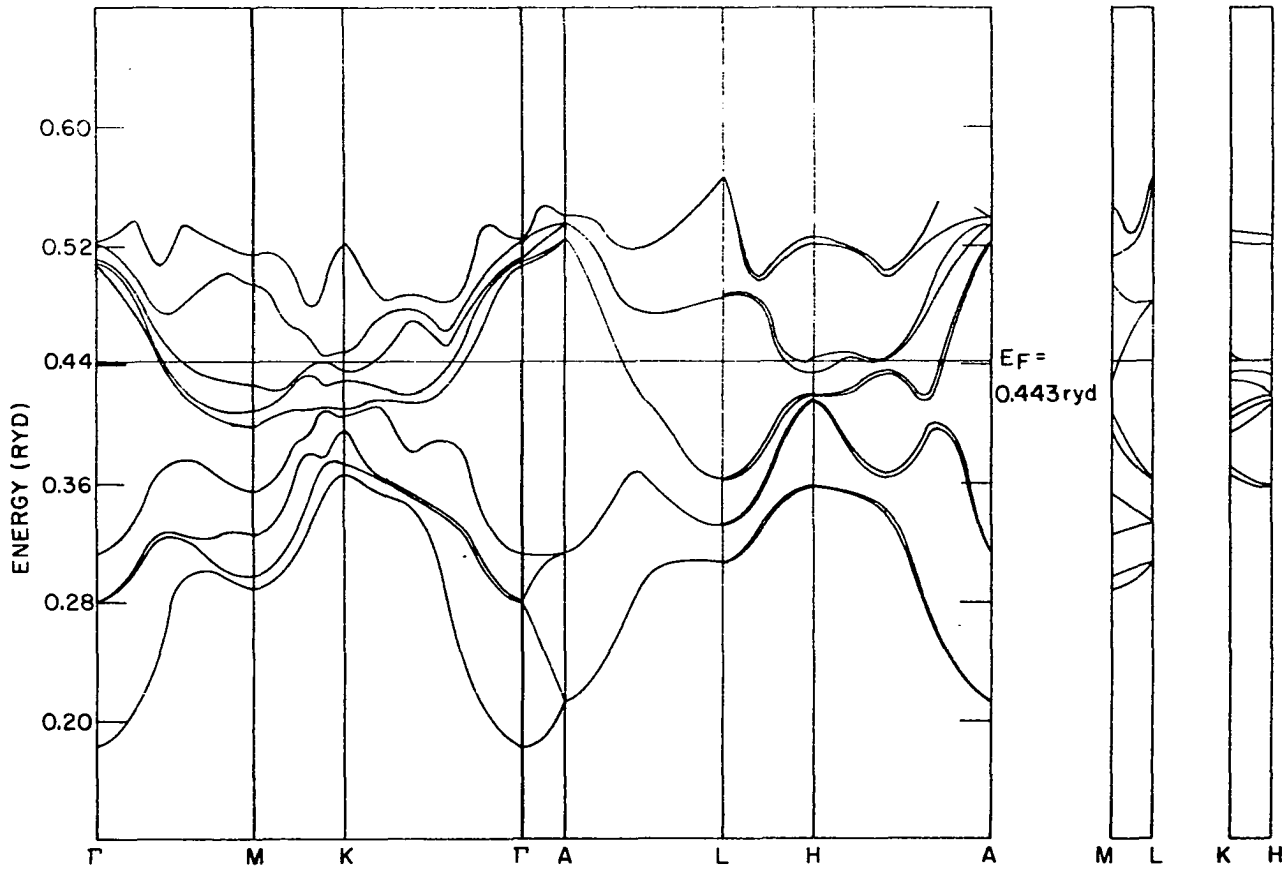

Figure 3. Relativistic energy bands for dhcp lanthanum

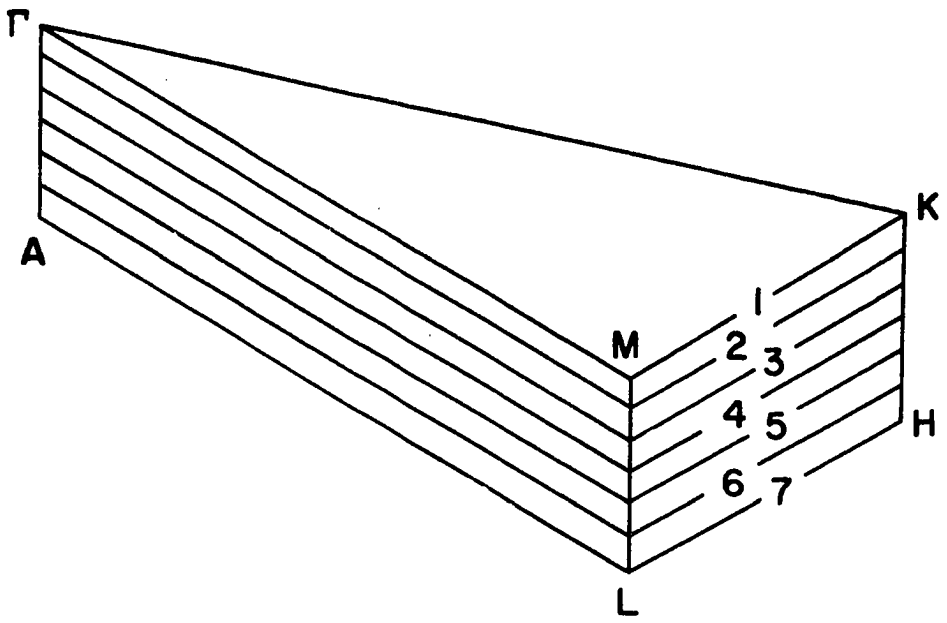

Figure 4. 1/24th Brillouin zone showing the seven layers in which energy eigenvalues were determined

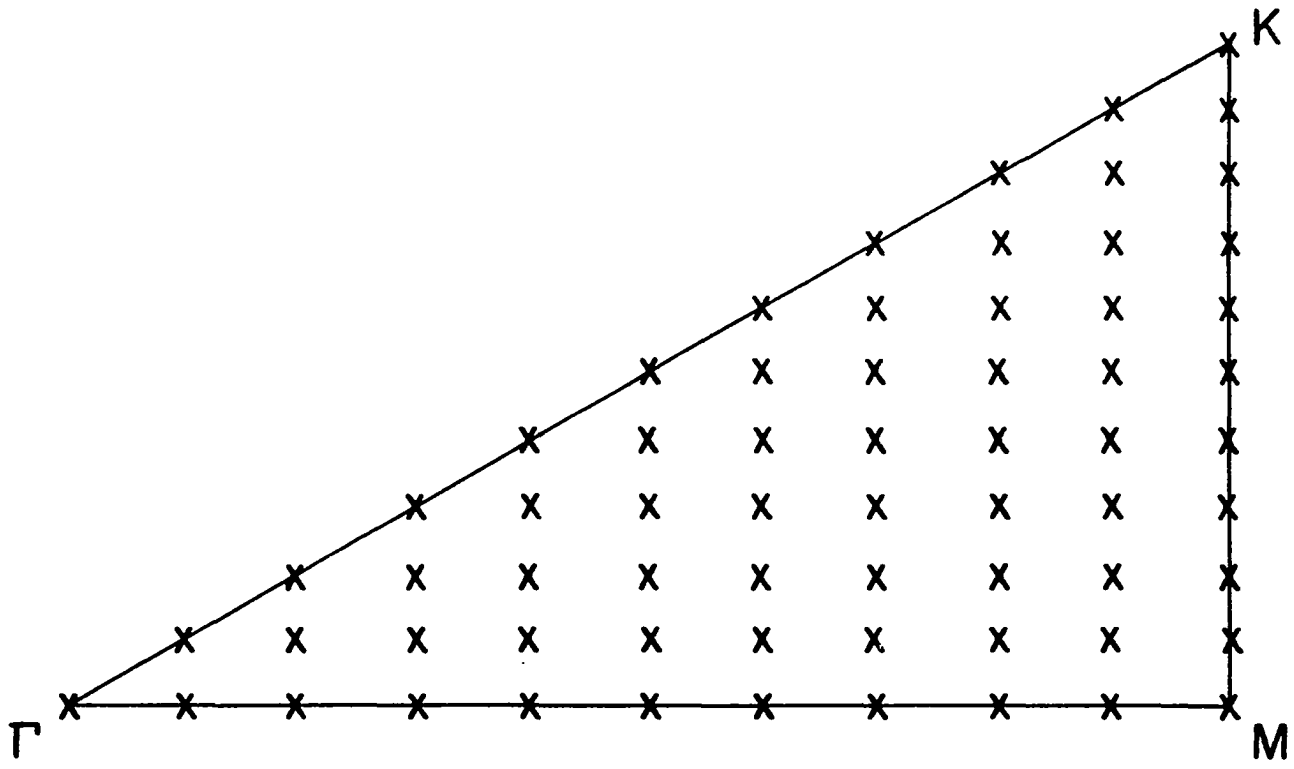

Figure 5. Cross section of the 1/24th zone showing points at which energy eigenvalues were determined

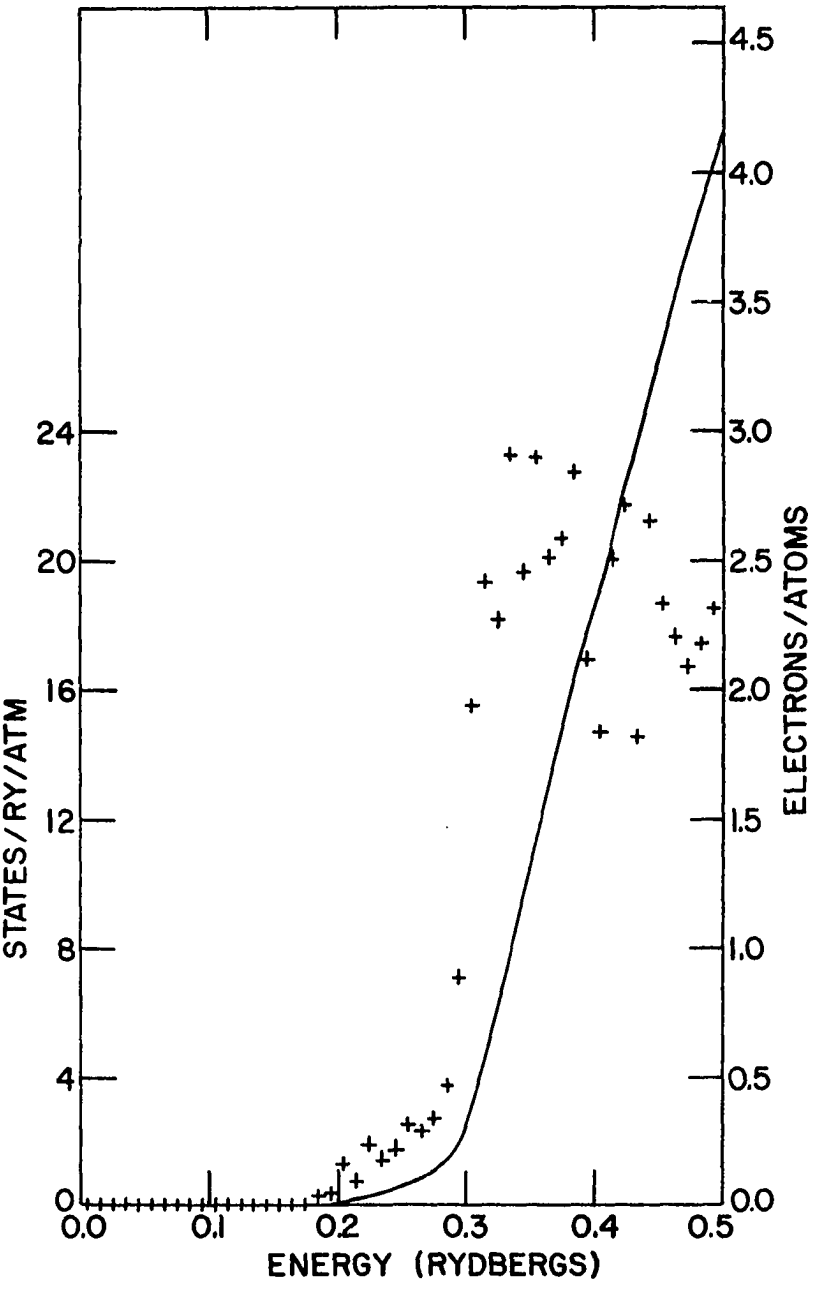

Figure 6. Density of states for lanthanum . The points represent the differential density of states (scale to left) and the solid curve is the integrated density of states (scale to right)

at .443 Ryd which is .253 Ryd above the bottom of the bands at Γ.

Table 3. Reciprocal lattice vectors used in the RAPW expansion for all points in the Brillouin zone

$(ijk) \equiv i\underline{k}_1 + j\underline{b}_2 + k\underline{b}_3$

	$(\bar{1}1\bar{4})$	$(\bar{1}0\bar{4})$	$(00\bar{4})$				
	$(\bar{1}1\bar{3})$	$(\bar{1}0\bar{3})$	$(00\bar{3})$	$(01\bar{3})$			
	$(\bar{1}1\bar{2})$	$(\bar{1}0\bar{2})$	$(00\bar{2})$	$(01\bar{2})$			
$(\bar{2}1\bar{1})$	$(\bar{1}1\bar{1})$	$(\bar{1}0\bar{1})$	$(00\bar{1})$	$(00\bar{1})$	$(01\bar{1})$	$(1\bar{1}\bar{1})$	$(10\bar{1})$
$(\bar{2}10)$	$(\bar{1}10)$	$(\bar{1}00)$	(000)	$(0\bar{1}0)$	(010)	$(1\bar{1}0)$	(100)
	$(\bar{1}11)$	$(\bar{1}01)$	(001)	$(0\bar{1}1)$	(011)	$(1\bar{1}1)$	(101)
	$(\bar{1}12)$	$(\bar{1}02)$	(002)	$(0\bar{1}2)$			
	$(\bar{1}13)$	$(\bar{1}03)$	(003)				

If a smooth curve is drawn for the density of states the value of the density of states at the Fermi energy is found to be 19.4 states/Ryd/atom. This value includes a factor of 2 so as to count both spin states. A recent experimental determination of the density of states in La was made by Johnson and Finnemore (1967) who found $N(E_F)$ to be 27.2 states/Ryd/atom. McMillan (1968) has shown that electron-phonon interaction can account for the difference between this value and that which we have calculated. Using the data of Johnson and Finnemore in McMillan's equation the density of states at the Fermi energy becomes 17.7 states/Ryd/atom which is within the spread of the points shown in Figure 6.

E. Energy Bands for Neodymium and Praseodymium

Following lanthanum in the periodic table come Ce(Z = 58), Pr(59) and Nd(60) which also have dhcp crystal structures. As has been mentioned earlier this discussion will not include Ce because of difficulties with the 4f levels. For Pr and Nd which have free atom electronic configurations $4f^3 6s^2$ and $4f^4 6s^2$ respectively, the 4f levels have dropped below the Fermi energy and again have little effect on the Fermi surface and are not calculated. The free atom configurations are used instead of the metallic configurations which have one less 4f electron and one 5d electron because the charge densities for the latter have not been calculated by either Liberman, et al., (1965) or Herman and Skillman, (1963). It was shown by Keeton and Loucks (1968) that for the heavy rare earths the two different charge densities (metallic and free atom) produce only very minor changes in the energy bands. It is assumed that the charge densities used here produce realistic energy bands for metallic neodymium and praseodymium.

The bands were calculated using the same procedure as described for lanthanum. The Pr and Nd bands along high symmetry directions are shown in Figures 7 and 8 and the density of states curves in Figure 9 and 10. The Fermi energy for Pr is .518 Ryd (.329 Ryd above the bottom of the bands) while that for Nd is .510 Ryd (.320 Ryd from bottom).

The density of states at the Fermi energy was determined to be 16.2 for Pr and 16.8 for Nd. The most reasonable estimate of the density of states from experimental data can be made using the electronic specific heat data given by Gschneidner (1965).

From these data $N(E_F)$ is found to be 21.1 states/Ryd/atom for Pr and 24.9 states /Ryd/atom for Nd. Assuming that the electron-phonon interaction

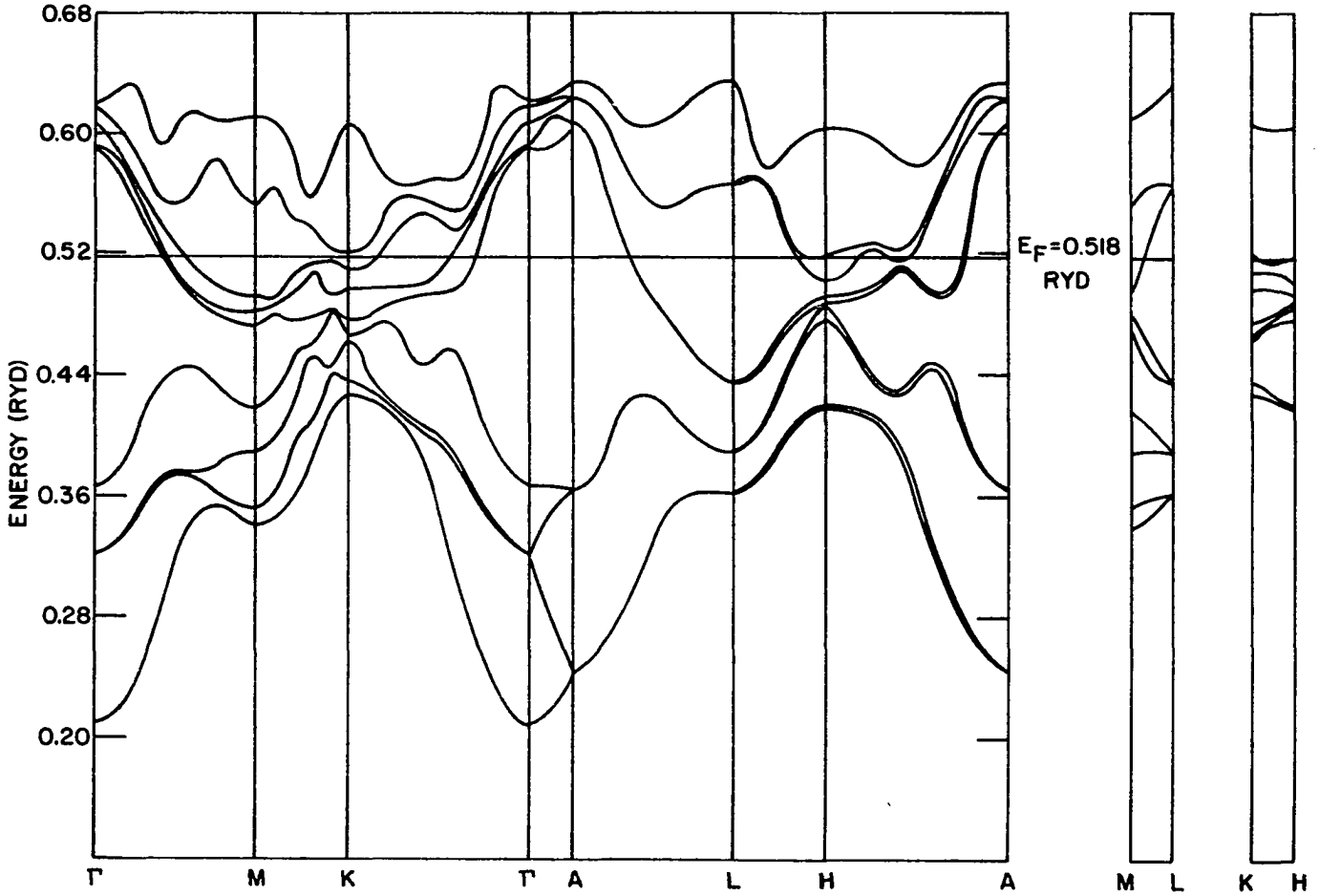

Figure 7. Relativistic energy bands for praseodymium

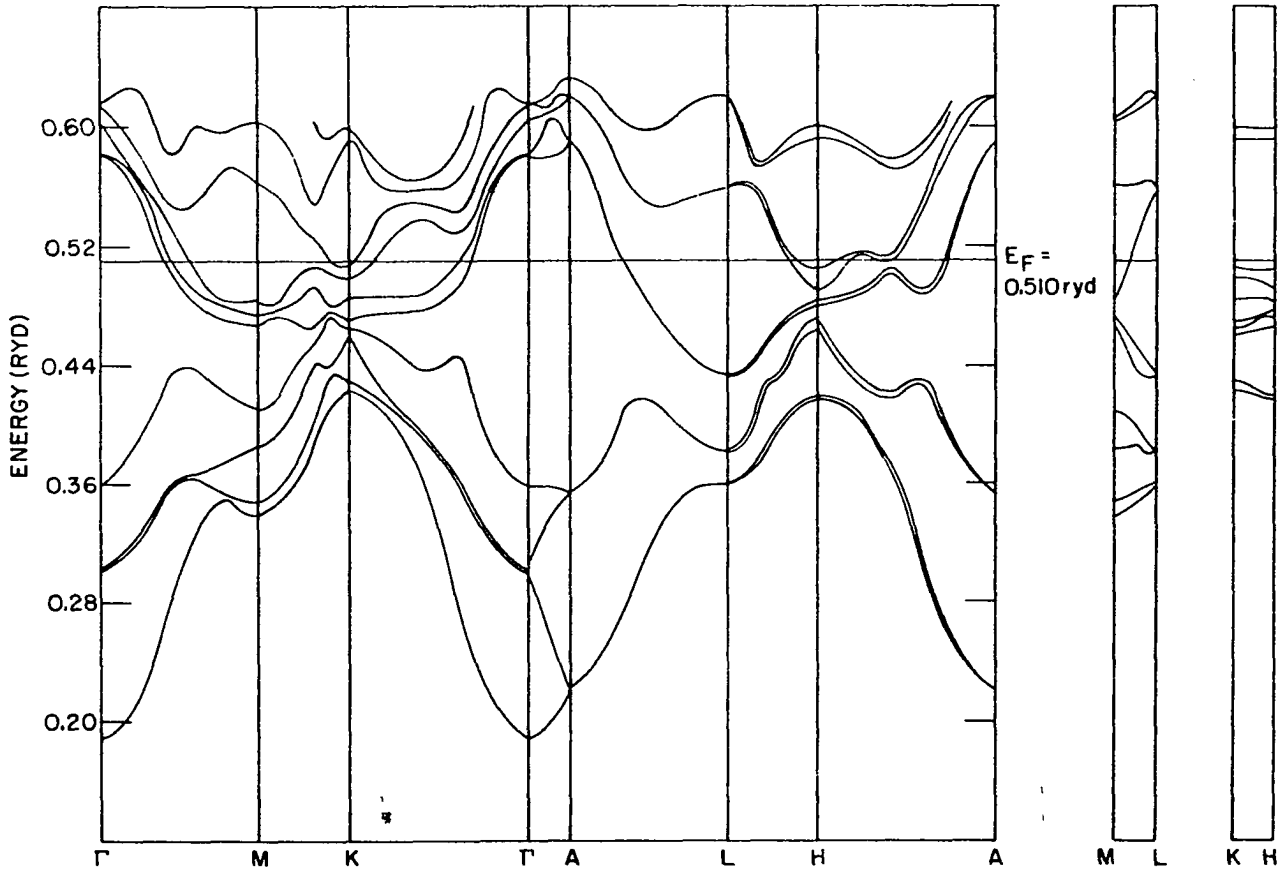

Figure 8. Relativistic energy bands for neodymium

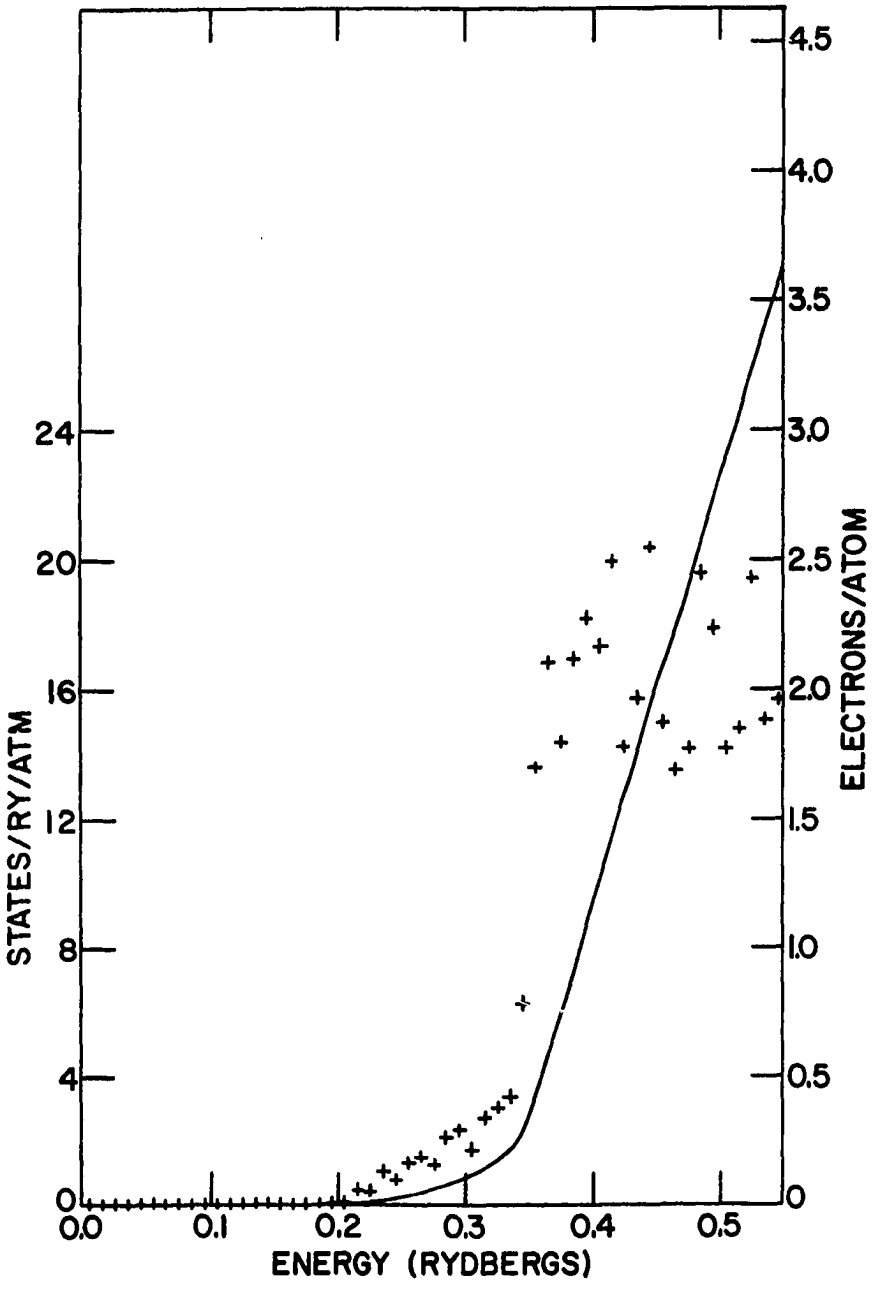

Figure 9. Density of states for praseodymium. The points represent the differential density of states (scale to left) and the solid curve is the integrated density of states (scale to right)

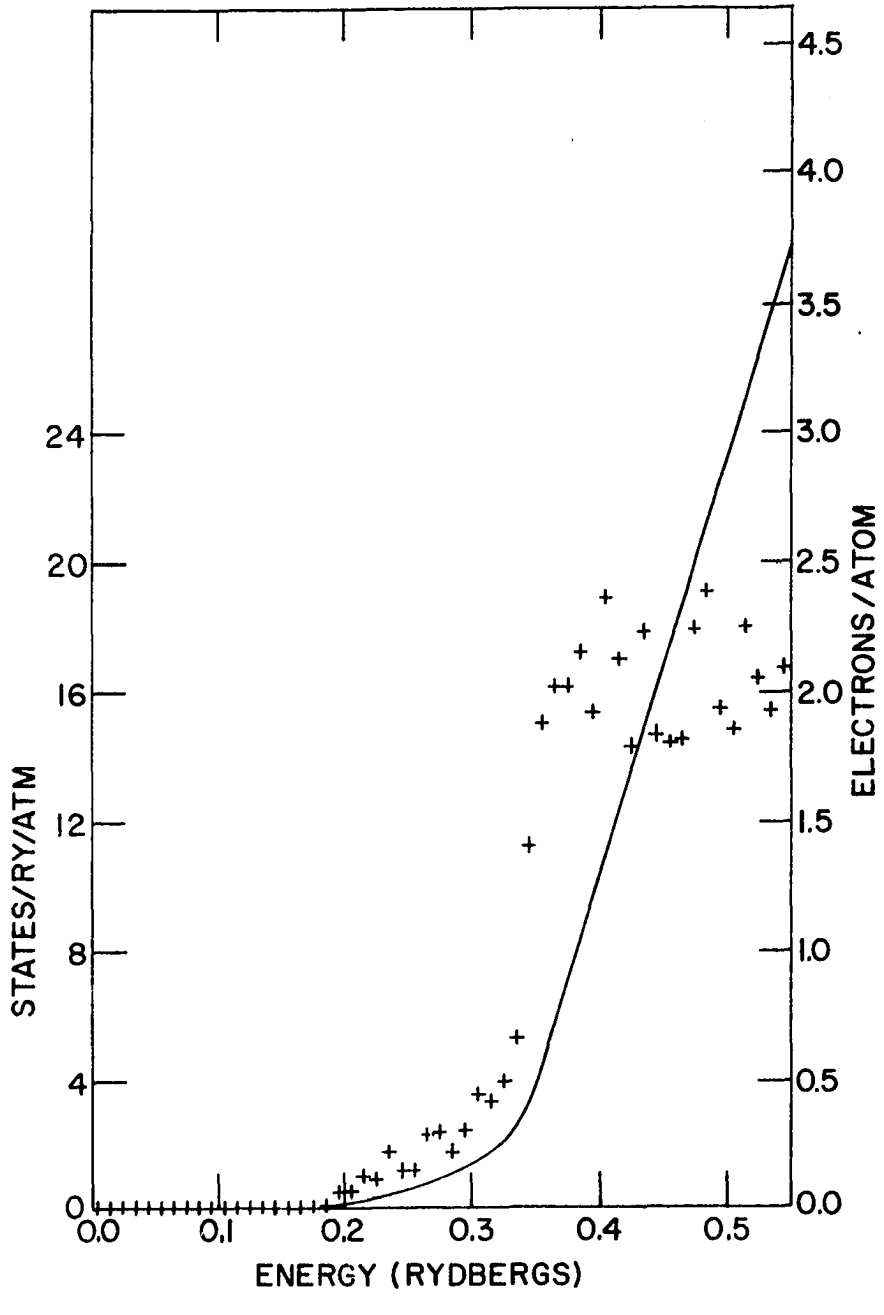

Figure 10. Density of states for neodymium. The points represent the differential density of states (scale to left) and the solid curve is the integrated density of states (scale to right)

correction is of the same order of magnitude as for La it is evident that the band densities of states will again be in reasonable agreement with those values which are calculated from the bands presented here.

IV FERMI SURFACE CALCULATIONS

A. Fermi Surfaces for La, Nd and Pr

Since the unit cell for a double hexagonal close-packed crystal is twice as large as that for a simple hcp crystal and contains four atoms instead of two, it is necessary that there be twice as many states per unit volume of reciprocal space. This not only demands that six bands be filled for a trivalent rare-earth element instead of three but it also implies that twice as many bands intersect the Fermi energy as for a simple hcp metal. Thus there are four bands which contribute to the Fermi surface rather than two as in the heavy rare-earth metals.

It would be convenient to represent the Fermi surface in a four zone scheme similar to the double zone scheme used for hcp metals (Freeman, et al., 1966) and the region of k space occupied by electrons of a given band could be easily shown. If it were not for spin-orbit coupling effects being included in the band calculations the structure factor at zone faces corresponding to the (001), (002) and (003) reciprocal lattice vectors would be continuous across these faces.

The inclusion of spin-orbit effects splits the bands (Falicov and Cohen, 1962) at all AHL zone boundaries and at alternate ΓKM faces and thus a Fermi surface in the four zone scheme would have discontinuities at these locations. It is therefore necessary to present the four pieces of the Fermi surface due to the four bands in the first zone. This makes the surface more difficult to represent than for a simple hcp metal since there are many regions in the zone which are occupied by electrons of all four bands. The representation can be simplified by showing the unoccupied or

hole regions from the fifth and sixth bands and the occupied or electron regions from the seventh and eighth bands. In all of the Fermi surface drawings shown in this section the fifth zone hole region will be shown darkly shaded and the sixth zone hole region lightly shaded. The seventh zone electron sections will be represented by diagonal lines and eighth zone electrons by the cross-hatched areas.

The intersections of the lanthanum Fermi surface with the faces of the 1/24th zone are shown in Figure 11 and with each of the seven layers in the zone for which energy eigenvalues were calculated are shown in Figure 12. Similar drawings of the neodymium and praseodymium Fermi surfaces are shown in Figures 13 through 16.

These surfaces share many common features and differ only in four details. All have a nearly circular column of fifth zone hole surface having a radius of approximately $.18b_1$ centered along the ΓA axis. The sixth zone hole surface is also centered along this axis. It tapers from a nearly hexagonal cross-section with faces separated by about $.4b_1$ in the ΓKM plane to a circular cross-section with an approximate diameter of $.36b_1$ at the AHL plane.

The seventh zone electron surface has a nearly circular cross-section centered at H in the AHL plane and extends outward roughly parallel to the KMHL plane as it approaches K and then about two-thirds of the distance from K to H extends out into a shelf which is centered about M when it intersects the ΓKM plane in the 1/24th zone. The eighth zone surfaces of the three elements have a small but very important difference. In La and Pr the major portion of this surface is an ellipsoid with its major axis lying along HK but in Nd the region extends the entire distance from H to K and is more

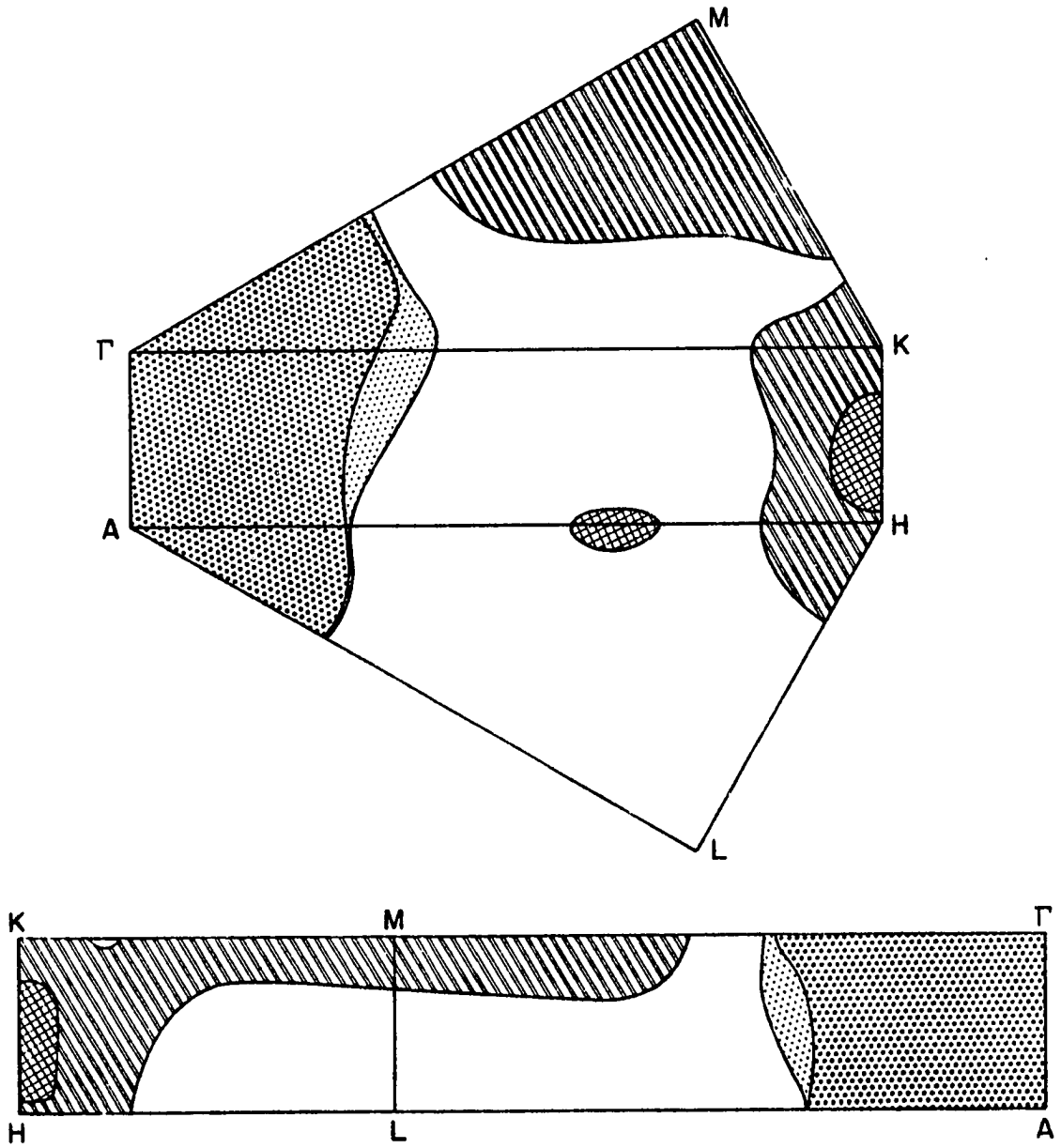

Figure 11. Intersections of the lanthanum Fermi surface with the faces of the 1/24th zone

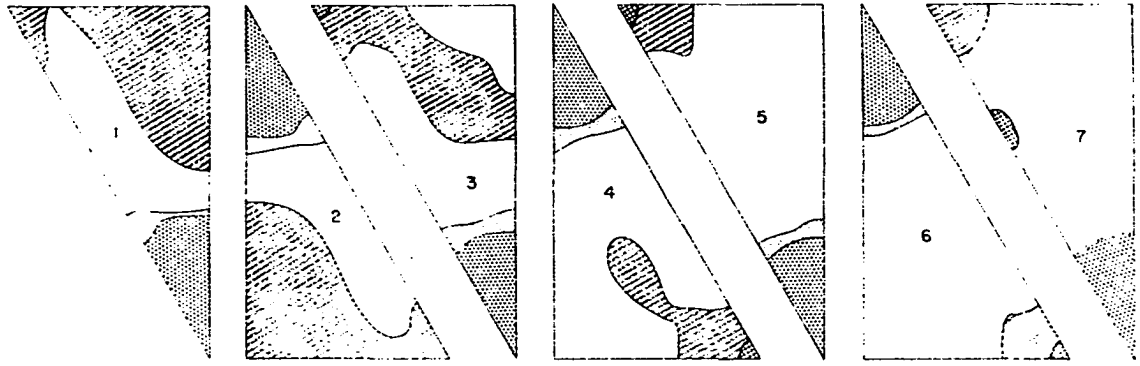

Figure 12. Cross sections of the lanthanum Fermi surface in each of the layers shown in Figure 4

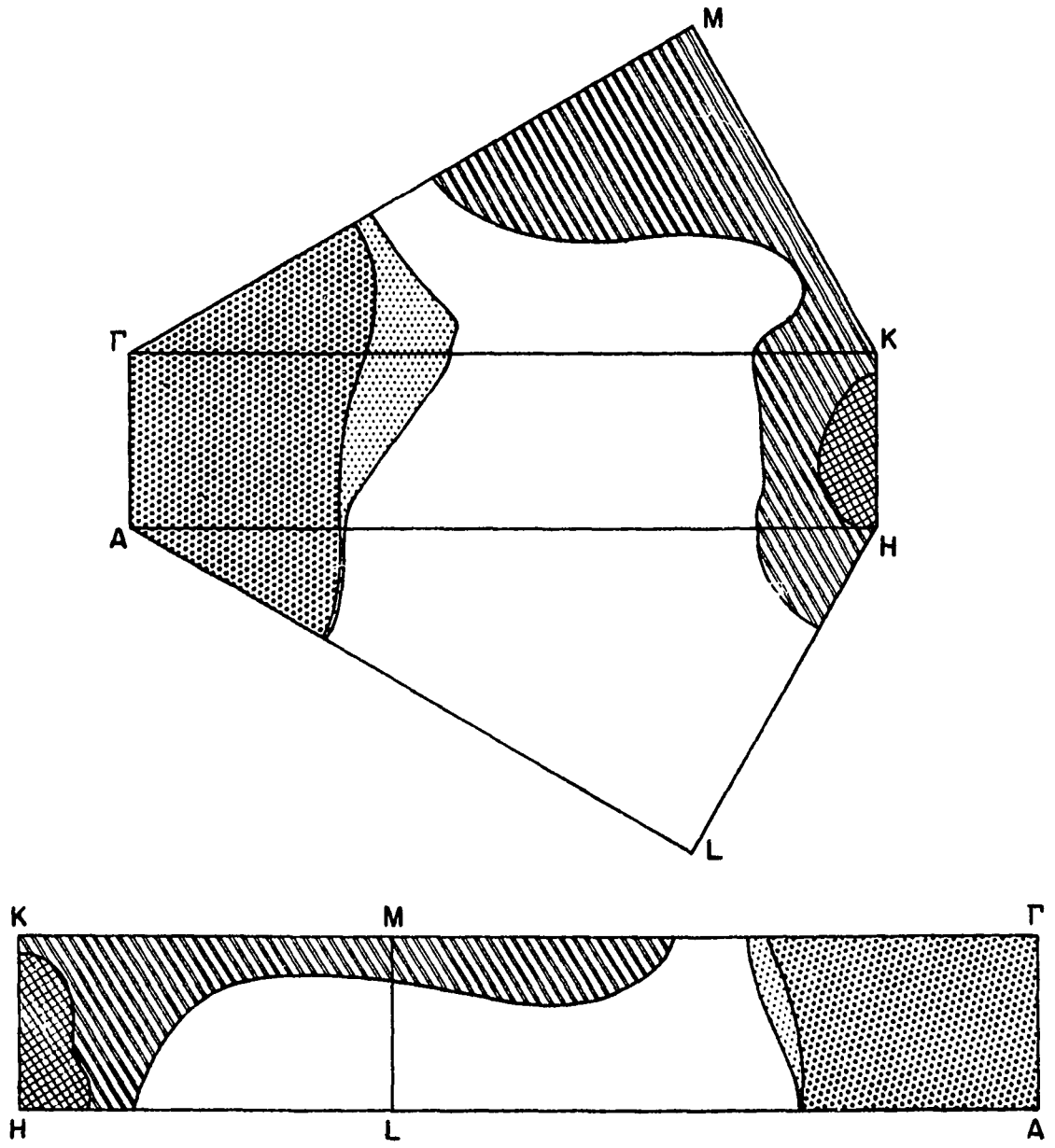

Figure 13. Intersections of the praseodymium Fermi surface with the faces of the 1/24th zone

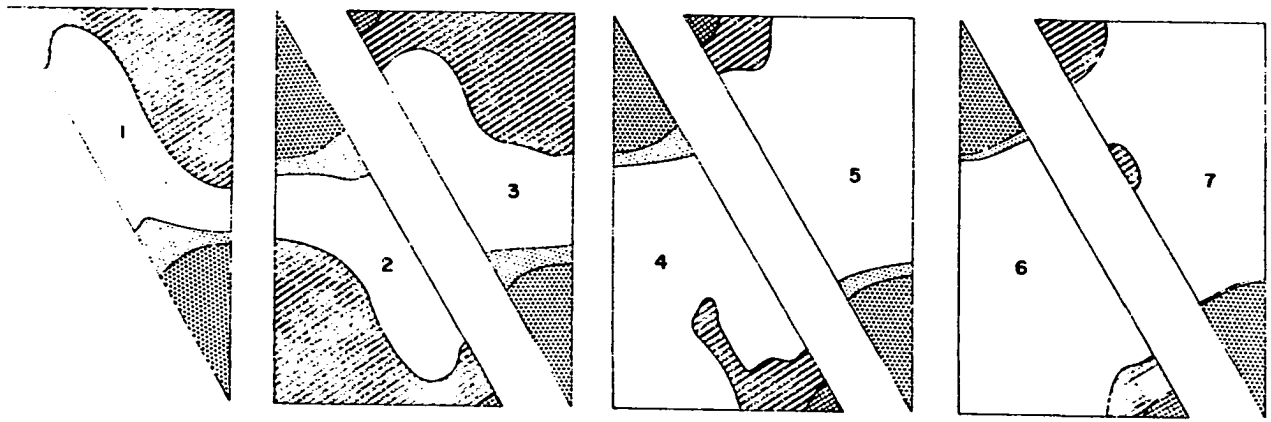

Figure 14. Cross sections of the praseodymium Fermi surface in each of the layers shown in Figure 4

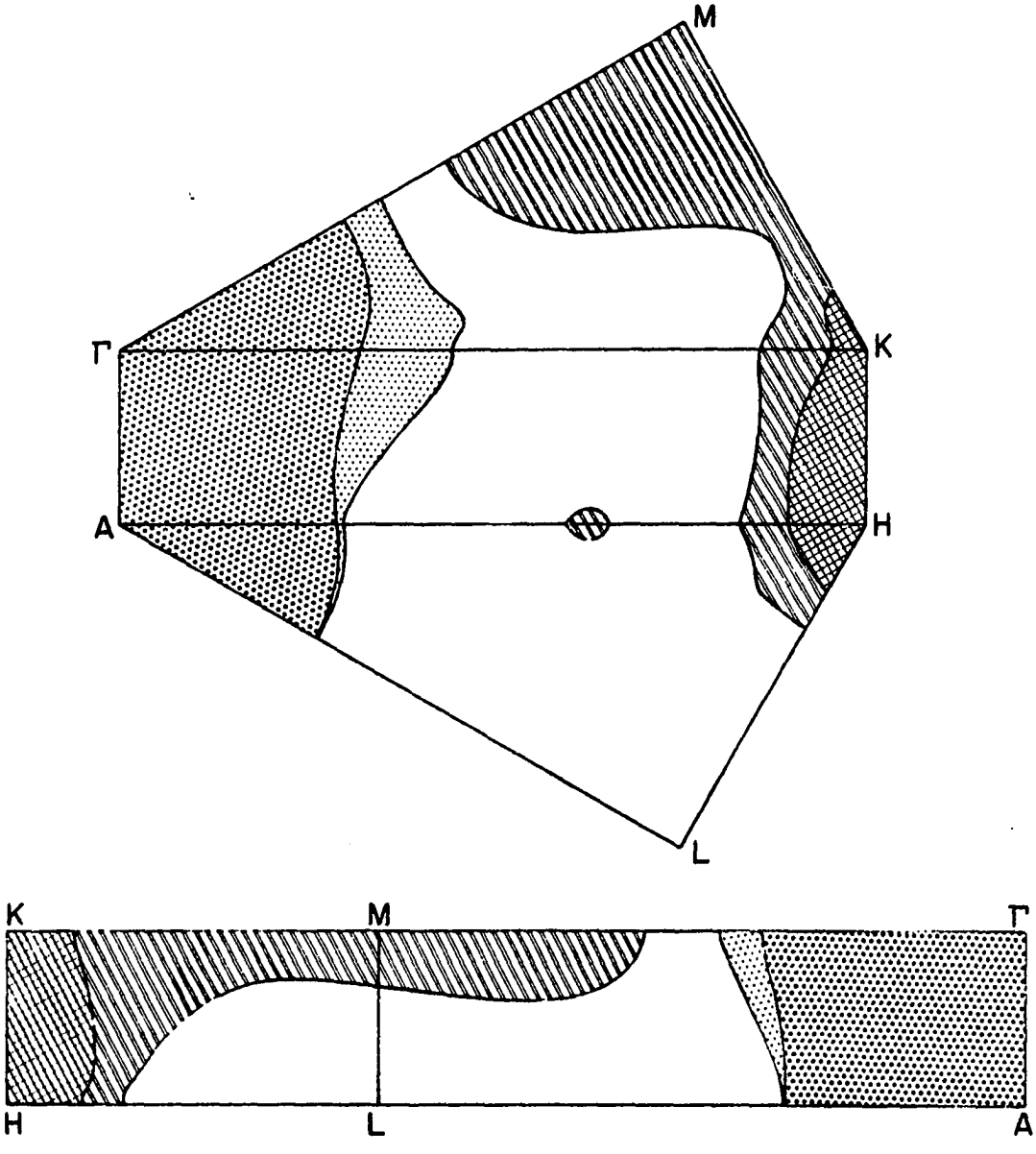

Figure 15. Intersections of the neodymium Fermi surface with the faces of the 1/24th zone

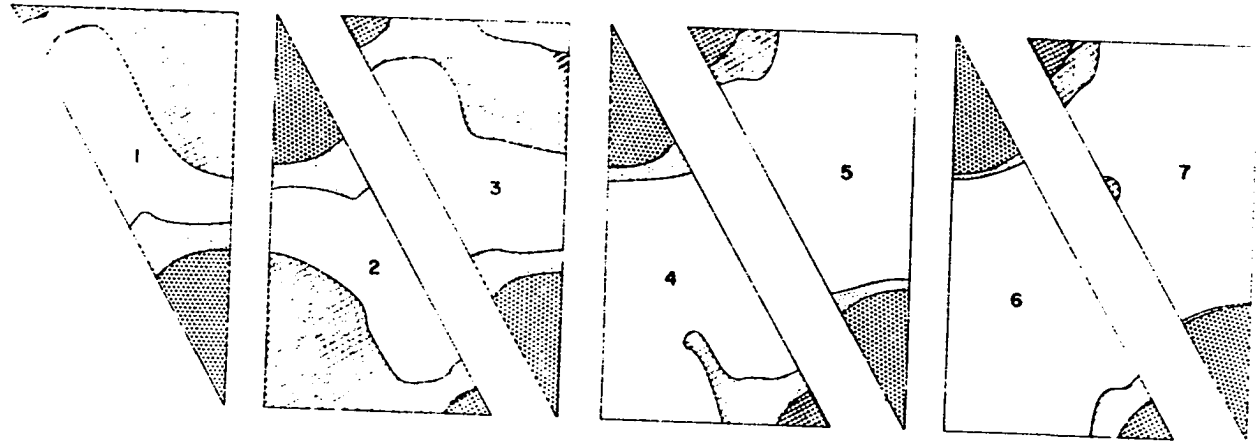

Figure 16. Cross sections of the neodymium Fermi surface in each of the layers shown in Figure 4

closely described as a cylinder along this axis with a cross-section shaping from elliptical at the ΓKM plane to nearly circular at the AHL plane. In addition in all of these metals there are small pockets of seventh and eighth zone electron surface lying along the AH axis.

B. Relationship of the Fermi Surfaces and the DHCP Crystal Structure

A very distinguishing feature of these Fermi surfaces is the absence of large, very flat pieces perpendicular to the c direction. In the work of Keeton and Loucks (1968) it was shown that such pieces are present for the heavy rare-earth metals and are located about half way between the center (the ΓKM face) and the edge (AHL) of the Brillouin zone. This missing feature of these Fermi surfaces appears to be strongly related to the existence of the dhcp crystal structures.

If in the crystal there exists a periodic potential with a propagation vector lying along the c-axis and having a period equal to twice the periodicity of the simple hcp lattice, this could introduce the necessary perturbation to eliminate these flat pieces of Fermi surface and reduce the total energy of the crystal. In La, Pr and Nd the dhcp structure creates such a potential and, indeed, the flat pieces are eliminated. Thus these Fermi surfaces indicate the stability of the dhcp structure over the simple hcp arrangement.

V MAGNETIC ORDERING IN ND AND PR

A. Magnetic Structure of Nd and Pr

The magnetic structures of the light rare-earth elements neodymium and praseodymium have been determined by neutron diffraction measurements made at Oak Ridge National Laboratory. Moon, et al., (1964) found by single crystal neutron diffraction that the first ordering of the magnetic moments in Nd occurs at 19K and that in the temperature range from 7.5K to 19K the magnetic moments ordered as shown in Figure 17a. There is no ordered moment on the sites (A) with fcc nearest neighbor symmetry but the moments on the sites with HCP symmetry are ordered antiferromagnetically between adjacent layers (B and C) with a sinusoidal modulation of the moments in each layer. Both the moments and the propagation vectors for the modulation lie along one of the equivalent $\underline{b}_1$ directions of the reciprocal lattice. The moments on the B and C sites are given by

$$\underline{\mu}_B = -\underline{\mu}_C = \underline{\mu}_1 \cos(2\pi \underline{Q}_1 \cdot \underline{\chi}) \tag{24}$$

where

$$\underline{\mu}_1 = (2.3 \pm 0.2)\left(\sqrt{\frac{3}{2}}\,\hat{i} + \frac{1}{2}\,\hat{j}\right)\mu_B \tag{25}$$

where μ_B is the Bohr magneton and $\underline{Q}_1$ lies along the $\underline{b}_1$ direction with a magnitude varying from $.13b_1$ at 18K to $.11b_1$ at 8K.

At temperatures below 7.5K there is also ordering of the moments on the A(fcc) sites. The arrangement of moments is as shown in Figure 17b with the moments in the B and C layers ordered in the same manner as for the higher temperature range and the moments in the 4 layers aligned in the $\hat{i}$ direction with a sinusoidal modulation with a propagation vector parallel

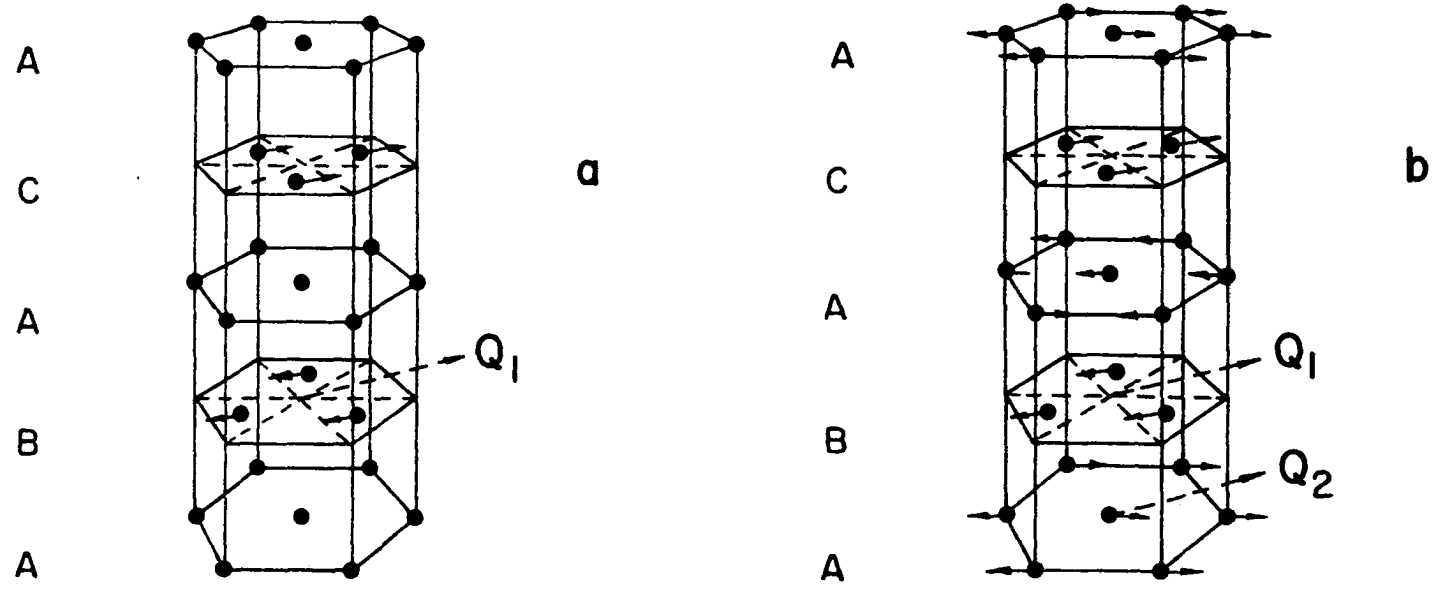

Figure 17. Magnetic structure of neodymium for (a) $7.5 < T < 19K$ and (b) $T < 7.5K$

to the vector for the fcc ordering. These moments can be expressed as

$$\underline{\mu}_{A1} = -\underline{\mu}_{A2} = \mu_2 \hat{i} \cos(2\pi \underline{Q}_2 \cdot \underline{X}) \tag{26}$$

where

$$\mu_2 = 1.8 \pm 0.2\mu_B \tag{27}$$

and $\underline{Q}_2$ lies along the $\underline{B}_1$ direction with a magnitude of $.15b_1$ at 1.6K.

It is important to note that in analyzing their data and constructing this model for the periodic moment arrangement Moon, et al. have assumed that the moments in the two sublattices do not interact. Koehler (1965) states that in order to account for all of the observed data it would be necessary to include a weak interaction between the moments on the hcp and fcc sites. However, the model described is sufficient to account for most of the observations and appears to be an excellent first approximation to the magnetic structure of Nd.

The magnetic structure of praseodymium has been determined by neutron diffraction measurements on polycrystalline samples (Cable, et al., 1964). Those data indicate that Pr has a magnetic structure similar to that observed for the first ordering in Nd. There is only one ordered phase in Pr which occurs at temperatures below 25K. The data can be interpreted in two possible ways (Koehler, 1965). Either all of the moments are ordered and have a magnitude of $0.7\mu_B$ or only the moments on one set of sites are ordered as in Figure 17a and the magnitude of the moments is $1.0\mu_B$. In either case the wave vector of the modulation is $.13b_1$ and it lies in the same direction as for Nd.

The important difference between these data is that there is only one ordered state for Pr while Nd has two different orderings with periodicities

described by different wave vectors. It should therefore be expected that because of the weak coupling between the two sublattices a theoretical investigation of the magnetic ordering should indicate a second ordering for Nd in addition to the basic ordering which occurs in both metals.

B. Theory of Magnetic Ordering: Indirect Exchange

The rare-earth metals with the exception of lanthanum and lutecium have partially filled 4f electron shells which according to Hund's rules will have a net magnetic moment J. For these metals the 4f electrons are very localized and there is negligible overlap between 4f electrons of neighboring atoms. Thus it is impossible for the Heisenberg exchange between 4f electrons to occur and produce any magnetic ordering. However, exchange between neighboring 4f shells can occur indirectly and produce the observed ordering in the following manner. Because the 4f wave functions overlap the conduction electron (6s) wave functions, it is possible for the 4f spin to polarize the nearby conduction electron spins via the s-f exchange interaction. The conduction electrons form a spin density wave (SDW), a long-range oscillatory polarization (Overhauser, 1963). The resultant polarization of the conduction electrons in the vicinity of another ion will then interact with the moment of that 4f shell and align its moment. Thus if the wavelength of the dominant mode of the spin density wave equals the atomic separation in the crystal the moments will align parallel; and if it is twice the atomic separation, nearest neighbor moments will align antiparallel to each other. In general the SDW wavelength will not be commensurate with the lattice and some type of a sinusoidally modulated periodic moment arrangement (PMA) results.

This indirect exchange mechanism was first proposed by Ruderman and Kittel (1954) in connection with nuclear magnetic resonance and was later extended to explain s-d and s-f interactions in magnetic materials by Kasuya (1956) and Yosida (1957). This model has become known as the Ruderman-Kittel-Kasuya-Yosida (RKKY) interaction and has been used extensively to account for both ferromagnetic and antiferromagnetic ordering in solids.

A fine derivation of the effective Hamiltonian for the RKKY interaction is given by Mattis (1965). In this treatment the perturbation Hamiltonian due to exchange coupling between two localized moments $\underline{S}_1$ and $\underline{S}_2$ located at $\underline{R}_1$ and $\underline{R}_2$ and the conduction electrons is given by

$$H = -J[\underline{S}_1 \cdot \underline{s}(\underline{R}_1) + \underline{S}_2 \cdot \underline{s}(\underline{R}_2)] \tag{28}$$

where J is the direct exchange coupling constant and $\underline{s}(\underline{R})$ is the conduction-band spin operator. Substituting the Bloch operators for the conduction-band spin operators and then using perturbation theory, the first non-vanishing correction to the energy is

$$E_t^{(2)} = -\frac{1}{4N^2} \sum_{\underline{k}\underline{k}'} J^2(\underline{k},\underline{k}') \frac{(t|s_1(s_1+1)+s_2(s_2+1)+2\underline{S}_1 \cdot \underline{S}_2 \cos(\underline{k}-\underline{k}') \cdot \underline{R}_{12}|t)}{E(\underline{k}') - E(\underline{k})} \cdot$$

$$f_{\underline{k}}(1 - f_{\underline{k}'}) \tag{29}$$

where the state $|t)$ is one of the $(2s_1+1)(2s_2+1)$ states of solute spins and $J(\underline{k},\underline{k}')$ is the exchange integral which is dependent on the wave vectors $\underline{k}$ and $\underline{k}'$. The Fermi function for wave vector $\underline{k}$ is $f_{\underline{k}}$. The first two terms in the matrix element represent the self energies of the two spins and are independent of their orientation. The last term is the energy of the inter-

action between the two spins. The interaction Hamiltonian for this system can be written as

$$H_I = - \sum_{i,j} J_I(\underline{R}_{ij}) \underline{S}_i \cdot \underline{S}_j \tag{30}$$

where now instead of considering two spins the sum is over all of the pairs of solute spins in the system. The indirect exchange coupling constant is given by

$$J_I(\underline{R}_{ij}) = \frac{1}{N^2} \sum_{\underline{k}\underline{k}'} J^2(\underline{k},\underline{k}') \frac{f_{\underline{k}}(1 - f_{\underline{k}'})}{E(\underline{k}') - E(\underline{k})} e^{i(\underline{k}-\underline{k}')\cdot\underline{R}_{ij}} \tag{31}$$

Assuming that the solute spins are points and only interact with the conduction electrons over an infinitesimally small region the exchange integral becomes independent of the wave vector. Actually the charge clouds are of finite size and the approximation must be made that $J(\underline{k},\underline{k}') \simeq J$ (Liu, 1961). With this approximation the coupling constant can be written

$$J_I(\underline{R}_{ij}) = \frac{J^2}{N^2} \sum_{\underline{k}\,\underline{k}'} \frac{f_{\underline{k}}(1 - f_{\underline{k}'})}{E(\underline{k}') - E(\underline{k})} e^{i(\underline{k}-\underline{k}')\cdot\underline{R}_{ij}} . \tag{32}$$

It is convenient to define a generalized susceptibility, $\bar{\chi}(\underline{q})$ of the conduction electron system. The interaction of the conduction electrons with the solute spins yields the energy perturbation

$$H = - \frac{1}{2} \sum_{\underline{q}} \chi(\underline{q}) |H_{\underline{q}}|^2 \tag{33}$$

where $\underline{H}_{\underline{q}}$ is the Fourier transform of the effective field due to the spin $\underline{S}_i$ located at $\underline{R}_i$. The effective field can be written as

$$\underline{H}(\underline{R}_i) = \frac{J}{\mu_B} \underline{S}_i \tag{34}$$

and its Fourier transform is then

$$\underline{H}_{\underline{q}} = \frac{J}{\mu_B \sqrt{N}} \frac{1}{} \sum_i e^{-i\underline{q}\cdot\underline{R}_i} \underline{S}_i \tag{35}$$

where J is the exchange integral and now N is the number of solute spins in the crystal.

Substituting Equation 35 in Equation 33 gives the Hamiltonian

$$H = -\frac{J^2}{2\mu_B^2 N} \sum_{ij} \underline{S}_i \cdot \underline{S}_j \sum_{\underline{q}} e^{i\underline{q}\cdot(\underline{R}_i - \underline{R}_j)} \chi(\underline{q}) \tag{36}$$

Comparing Equations 36 and 30 it is easily seen that

$$J_1(\underline{R}_{ij}) = \frac{J^2}{2\mu_B^2 N} \sum_{\underline{q}} e^{-i\underline{q}\cdot\underline{R}_{ij}} \chi(\underline{q}) \tag{37}$$

and it is apparent that $\chi(\underline{q})$ differs from the Fourier transform of J_1 by only a constant multiple. Setting this constant equal to unity for convenience the generalized susceptibility can be written as

$$\chi(\underline{q}) = \sum_j J_1(\underline{R}_j)\, e^{i\underline{q}\cdot\underline{R}_j} \tag{38}$$

where $\underline{R}_j$ is the distance from a spin at the origin of the coordinate system. Substitution of Equation 30 into this expression gives

$$\chi(\underline{q}) = \frac{J^2}{N} \sum_{\underline{k}} \frac{f_{\underline{k}}(1 - f_{\underline{k}+\underline{q}+\underline{g}})}{E(\underline{k}+\underline{q}) - E(\underline{k})} \tag{39}$$

where the sum is over all k-space and not restricted to the first Brillouin zone and $\underline{g}$ is any reciprocal lattice vector.

Now it is of interest to see how the RKKY exchange and the generalized susceptibility relate to the most stable configuration of magnetic moments in a crystal. This relationship was obtained by Villain (1959) using a statistical mechanical approach and more recently by Nagamiya (1967) by

minimizing the Fourier transform of the exchange energy expression. This latter procedure will be followed here.

The Fourier transform of the RKKY exchange coefficient is

$$\underline{J}_{\underline{q}} = \sum_{n} J(\underline{R}_{ij}) e^{i\underline{q}\cdot\underline{R}_{ij}} \tag{40}$$

and the spin configuration can also be transformed to give

$$\underline{S}_{\underline{q}} = \frac{1}{\sqrt{N}} \sum_{i} \underline{S}_{i} e^{i\underline{q}\cdot\underline{R}_{i}} \quad . \tag{41}$$

Using these relationships the indirect exchange energy given in Equation 30 can be expressed as

$$H_{I} = - \sum_{q} J_{\underline{q}} \underline{S}_{\underline{q}} \cdot \underline{S}_{\underline{q}}^{*} \tag{42}$$

and the stable configuration will result when this summation is minimized subject to the constraints that $\underline{S}_{n}^{2}$ must be a constant. This constraint can be written in a weaker form as

$$\sum_{q} \underline{S}_{\underline{q}} \cdot \underline{S}_{\underline{q}}^{*} = \text{constant.} \tag{43}$$

It is immediately obvious that subject to this constraint H_{I} is minimized when there exists only one Fourier component of spin configuration, that for which $J_{\underline{q}}$ is a maximum and this value of $\underline{q}$ shall be denoted as $\underline{Q}$. Taking the inverse of Equation 41 and writing it in component form gives the spin configuration of minimum energy

$$\begin{aligned} S_{ix} &= A \cos (\underline{Q} \cdot \underline{R}_{i} + \alpha) \\ S_{iy} &= B \cos (\underline{Q} \cdot \underline{R}_{i} + \beta) \\ S_{iz} &= C \cos (\underline{Q} \cdot \underline{R}_{i} + \gamma) \quad . \end{aligned} \tag{44}$$

There are many spin configurations which can meet these requirements. Some of the more common ones are the helical structure, antiferromagnetic or ferromagnetic, conical structures and sinusoidally modulated longitudinal moment arrangements. The configuration which a particular crystal will assume depends on factors not considered here such as anisotropy of the crystal field and magnetoelastic effects but all configurations have a common property. That is that the wave vector of the periodicity is the same wave vector for which the generalized susceptibility is a maximum.

C. Application of the Theory to Nd and Pr

The light rare-earth metals neodymium and praseodymium have partially filled 4f shells which are bound tightly to the individual atoms. The partially filled shell results in the ion core possessing the angular momentum given in Table 4. In addition the wave functions for the 4f electrons (Herman and Skillman,1963) shown in Figure 18 are nearly zero beyond half the nearest neighbor distance so there is almost no overlap between 4f shells of adjacent atoms. Thus it is apparent that the RKKY interaction is the mechanism by which exchange occurs in these metals.

Table 4. Electronic configurations and angular momenta of Pr and Nd

Metal	Z	electronic configuration	s	ℓ	j
Pr	59	$4f^2 5d^1 6s^2$	1	5	4
Nd	60	$4f^3 5d^1 6s^2$	3/2	6	9/2

The unit cell for the dhcp crystal contains four atoms and it is

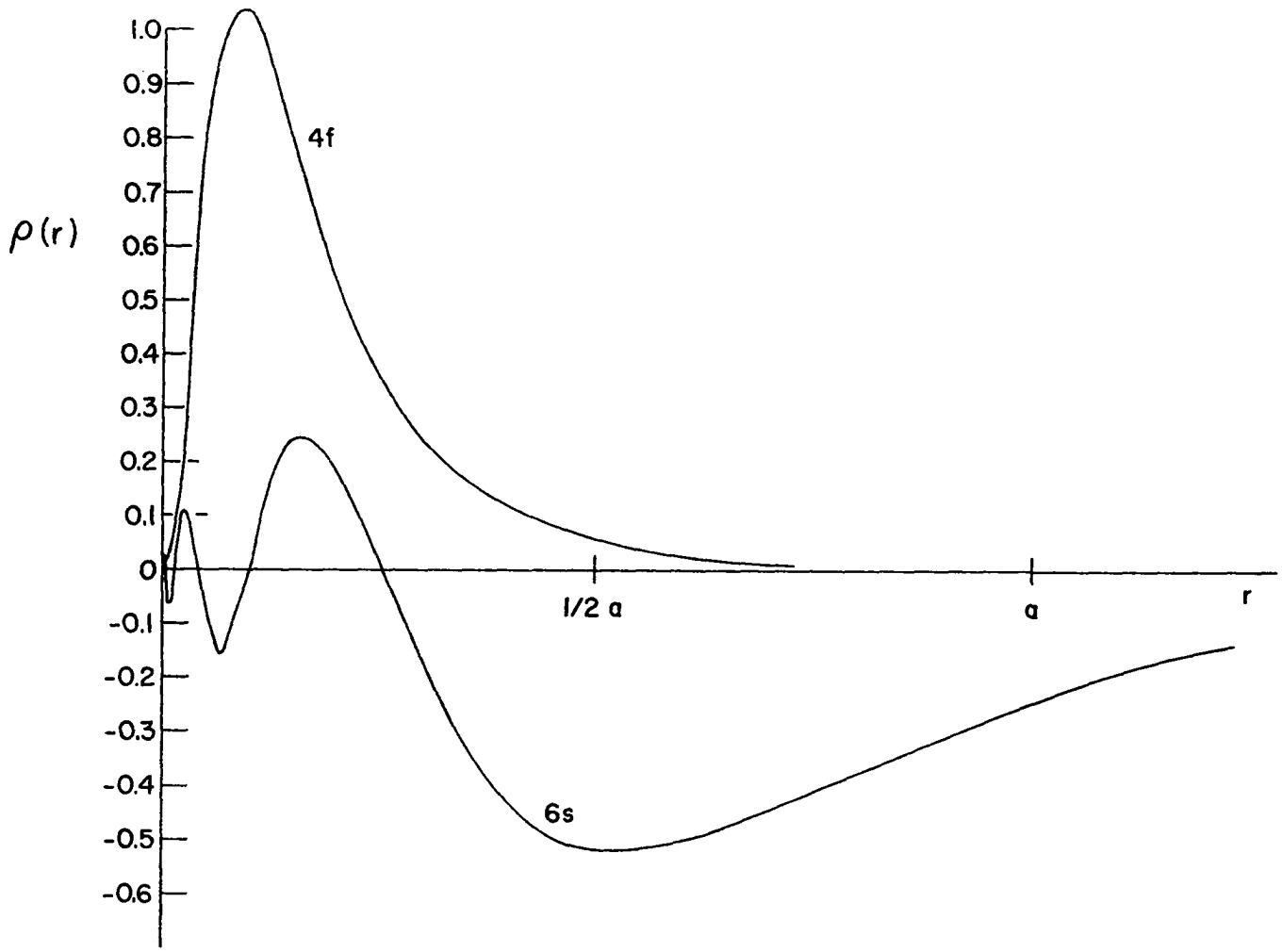

Figure 18. Wave functions for 6s and 4f electrons in neodymium

necessary to define four different Fourier transforms of the exchange parameter. In each case the transform will include a sum over the N unit cells of the crystal but only includes the equivalent atom in each cell. Letting the subscript ν represent a particular atom in the unit cell then four susceptibilities can be defined by

$$\chi_\nu(\underline{q}) = \sum_j J_1(\underline{R}_j + \underline{\rho}_\nu)\, e^{i\underline{q}\cdot(\underline{R}_j+\underline{\rho}_\nu)} \quad (\nu = 1,2,3,4) \tag{45}$$

where $\underline{R}_j$ is the vector to the jth unit cell and $\underline{\rho}_\nu$ is the vector in that cell to the νth atom. Substituting Equation 24 into this expression and using the result that

$$\sum_j e^{i(\underline{k}-\underline{k}'+\underline{q})\cdot(\underline{R}_j+\underline{\rho}_\nu)} = \frac{N}{4}\,\delta(\underline{k}+\underline{q}+\underline{g}-\underline{k}')e^{-i\underline{g}\cdot\underline{\rho}_\nu} \tag{46}$$

where $\underline{g}$ is a reciprocal lattice vector it follows that

$$\chi_\nu(\underline{q}) = \frac{J^2}{4N}\sum_{nn'}\sum_{\underline{k}} \frac{f_{n\underline{k}}(1 - f_{n'\underline{k}+\underline{q}+\underline{g}})}{E_n(\underline{k}+\underline{q}+\underline{g}) - E_n(\underline{k})}\, e^{-i\underline{g}\cdot\underline{\rho}_\nu} \tag{47}$$

where now the sum is over $\underline{k}$ in the first zone and the band indices n and n' with $\underline{g}$ the recip required the reduce $\underline{k}+\underline{g}$ to the first zone.

Since there are four atoms per unit cell in the dhcp crystal there are four branches of the generalized susceptibility in the primitive Brillouin zone. These four branches are defined by

$$\chi^{(1)}(\underline{q}) = \sum_\nu \chi_\nu(\underline{q})$$

$$\chi^{(2)}(\underline{q}) = \chi^{(1)}(\underline{b}_3 - \underline{q})$$

$$\chi^{(3)}(\underline{q}) = \chi^{(1)}(\underline{b}_3 + \underline{q})$$

$$\chi^{(4)}(\underline{q}) = \chi^{(1)}(2\underline{b}_3 - \underline{q}) \qquad (48)$$

where the magnitude of the component of the wave vector $\underline{q}$ along the c-axis is less than $1/2b_3$.

D. Relationship of Magnetic Ordering to Fermi Surfaces

It was shown earlier that the wave vector of the magnetic ordering periodicity is that for which the generalized susceptibility is a maximum. Examining Equation 31 it can be seen that a large contribution to $\chi(\underline{q})$ results when the energy of an occupied state, $E(\underline{k})$, is approximately equal to that of an unoccupied state, $E(\underline{k} + \underline{q})$. Since at low temperatures essentially all states below the Fermi energy are occupied and all above E_F are empty. This means that $E(\underline{k})$ must be slightly less than the Fermi energy or in other words $\underline{k}$ must lie just inside the Fermi surface and similarly $\underline{k} + \underline{q}$ must be slightly outside the Fermi surface.

There are many pairs of points which meet this requirement for any Fermi surface, but to get a large $\chi(\underline{q})$ there must be a large number of these pairs separated by the same wave vector $\underline{q}$. This implies that the required Fermi surface feature which will produce a maximum in $\chi(\underline{q})$ is the existence of two large flat parallel regions separated by the wave vector $\underline{q}$. Kasuya (1966) generated free electron bands in one, two and three dimensions to produce spherical, cylindrical and cubic Fermi surfaces and showed that the only case for which $\chi(\underline{q})$ had a maximum for non-zero $\underline{q}$ was for the cubic surface. In this case $\chi(\underline{q})$ became infinite for the wave vector separating two parallel faces of the cube.

Similar results have also been obtained for real metals. Lomer (1962)

first noticed that the wave vector separating flat parallel regions of the electron jack and hole octahedron of the chromium Fermi surface equalled that of the periodicity of the antiferromagnetic moment arrangement in the metal. Similar observations were made for heavy rare-earth metals by Dimmock and Freeman (1964), Anderson and Loucks (1968), Keeton and Loucks (1968) and Watson, et al., (1968). These observations were confirmed by Evenson and Liu (1968a) who used realistic energy bands for many of these elements to calculate their generalized susceptibilities. These results correctly predicted that Gd should be ferromagnetic while Dy, Ef, and Lu should have periodic moment arrangements with a wave vector along the $\underline{b}_3$ axis.

For Nd and Pr the principal flat pieces of Fermi surface are in the sixth and seventh zones. There is nesting of opposite faces of the hexagonal sixth zone piece which are separated by a wave vector $\underline{q} \simeq .38\underline{b}_1$. There are flat portions of seventh zone surface which nest into each other across the KHLM face of the zone and the wave vector for this separation is $\underline{q}_1 \simeq \underline{q}_2 \simeq .12\underline{b}_1$. Near the center of the 1/24th zone there are two regions of this seventh zone surface which have a separation $\underline{q}_3$ which is approximately equal to $\underline{q}_2$. All of these $\underline{q}$'s separate regions of the Fermi surface of a particular band and thus contribute to the first branch of the susceptibility. These wave vectors are shown in Figure 19.

There is one additional nesting which is more prominent in Nd than in Pr. This occurs between the seventh and eighth band electron surfaces across the KHLM zone face. The wave vector for this separation is $\underline{q} \simeq .10\underline{b}_1$ and the resulting maximum in susceptibility will be in the second branch of the $\chi(q)$ curve since this is an interband transition.

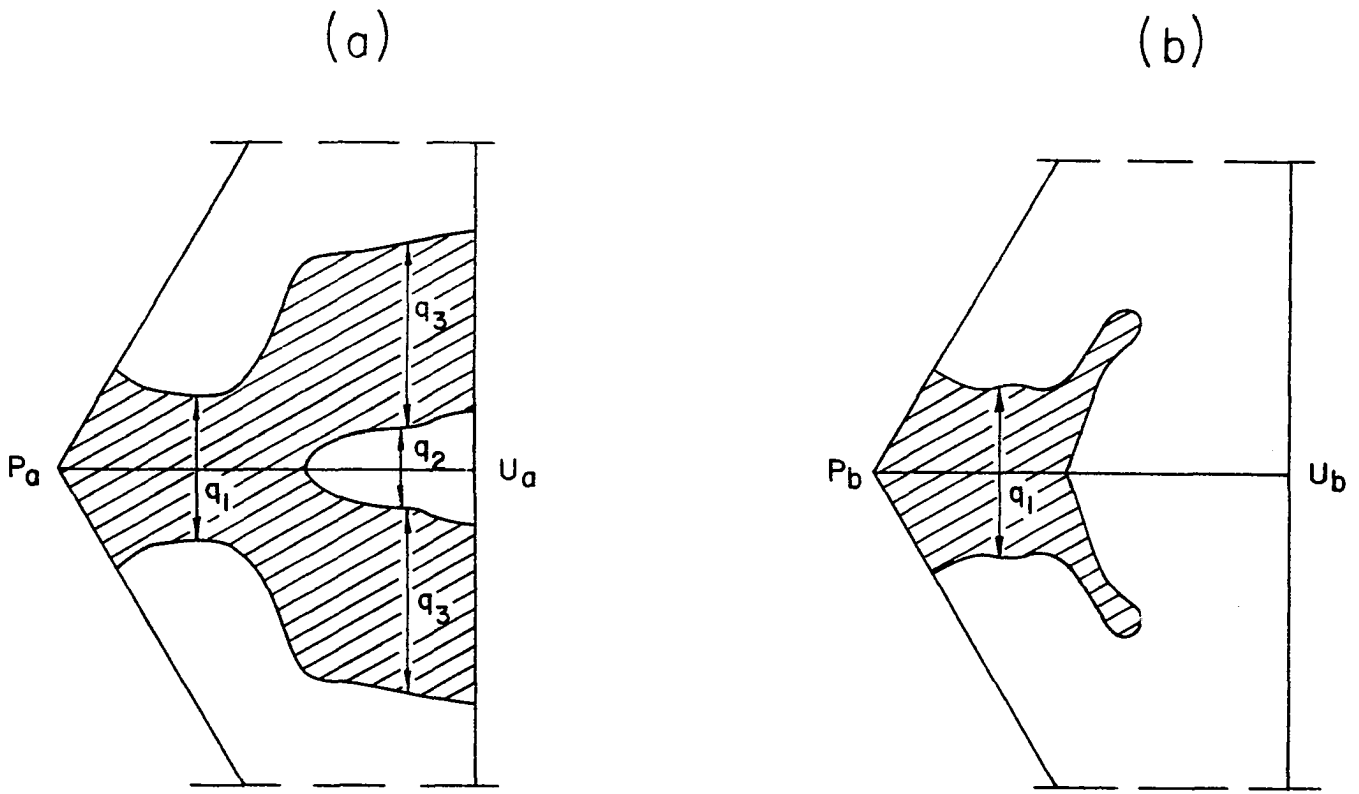

Figure 19. Cross sections of the Nd Fermi surface near the KMHL zone face for (a) $k_z = \frac{1}{6} b_3$ and (b) $k_z = \frac{1}{4} b_3$

The wave vectors initially used to describe all of these nesting features lay along the $\underline{b}_1$ direction in the reciprocal lattice since this is the direction in which the sinusoidal modulation of moments in these two metals occurs. However, on examination of the Fermi surfaces it appears that some or all of these wave vectors may have a $\underline{b}_3$ component in addition to that along $\underline{b}_1$. Thus it was decided to calculate $\chi(\underline{q})$ over the plane of $\underline{b}_1$ and $\underline{b}_3$ rather than just along $\underline{b}_1$. The results of these calculations are presented in the next section.

VI NUMERICAL CALCULATION OF THE GENERALIZED SUSCEPTIBILITIES FOR ND AND PR

A. Method of Calculation

From Equations 47 and 48 the generalized susceptibility for a dhcp metal can be written

$$\chi^{(1)}(\underline{q}) = \frac{J^2}{4N} \sum_{nn'\underline{k}} \frac{f_{n\underline{k}}(1 - f_{n'\underline{k}+\underline{q}+\underline{g}})}{E_{n'}(\underline{k}+\underline{q}+\underline{g}) - E_n(\underline{k})} \sum_{\nu=1} e^{-i\underline{g}\cdot\underline{\rho}_\nu} \tag{49}$$

The sum over the atoms of the unit cell is the same sum which occurred in the structure factor and was evaluated in Equation 13. The effect of the structure factor is to put a restriction on the bands between which transitions can occur. Assuming that the four bands which intersect the Fermi energy correspond to one band in an extended zone formed by folding out the bands in the $\underline{b}_3$ direction, the transitions allowed by the structure factor are from state $\underline{k}$ to state $\underline{k} + \underline{q}$ in this band.

The calculation of the total $\chi(\underline{q})$ should also include terms due to bands not intersecting the Fermi energy. It was shown by Evenson (1968) that these terms give a contribution to $\chi(\underline{q})$ which shift the $\underline{q}$ curve by a constant amount. Since it is the shape of the curve and location of the maximum value which is critical in determining the stable magnetic structure, the omission of these terms will not affect these results.

Since the wave vector $\underline{q}$ which will be used in these calculations will have a component in the $\underline{b}_1$ direction in addition to a $\underline{b}_3$ component, the effect of folding out the bands in the basal plane must also be considered. However, the magnitude of the basis vector $\underline{b}_1$ is 3.2 times greater than that of $\underline{b}_3$. As a result the separation of the bands produced by folding into

the single zone along the $\underline{b}_1$ aixs is considerably larger than the separation of the bands arising from a folding along the $\underline{b}_3$ axis. The contribution to the susceptibility is similar to that arising from transitions involving bands not intersecting the Fermi surface. Thus the only terms in the $\chi(\underline{q})$ sum which contribute significantly to the curve shape are those for which the reciprocal lattice vector $\underline{g}$ has no component in the basal plane, i.e. $\underline{g} = n\underline{b}_3$.

For the intraband transitions which give the significant contribution to $\chi(\underline{q})$ the structure factor equals 4 and Equation 41 can be written

$$\chi^{(1)}(\underline{q}) = \frac{J^2}{N} \sum_{\underline{k}} \frac{f_{\underline{k}}(1 - f_{\underline{k}} + q)}{E(\underline{k} + \underline{q}) - E(\underline{k})} \qquad (50)$$

where the sum is over the states $\underline{k}$ in the single band formed by folding out the four bands intersecting the Fermi energy into a four zone representation along the $\underline{b}_3$ direction.

The sum was then performed using a mesh of 14,400 uniformly spaced points $\underline{k}$ in the Brillouin zone. This mesh consisted of 1200 points in each of layers in which energy eigenvalues had been previously computed. The eigenvalues at those points for which a value had not been computed were determined by the same spline interpolation method used to obtain the points used in the density of states calculation. The separation between points in the $\underline{b}_1$ direction was $b_1/40$ and for the orthogonal direction $(\underline{b}_1 \times \underline{b}_3)$ in each plane the separation was $b_1/20\sqrt{3}$. The spacing between the k_z layers was $b_3/12$ which approximately equalled the other two spacings since $c/a \simeq 3.2$ for these metals.

In the derivation of the generalized susceptibility the matrix elements $J^2(\underline{k}, \underline{k}')$ were assumed to be constant. This approximation was based on the

assumption that the interaction of the 4f electrons with the conduction electrons occurred only at the points where the ions were located. However, the 4f shells do have finite size and the conduction electron polarization will have more oscillations within this shell as $|\underline{k} - \underline{k}'|$ increases. This causes the matrix elements to decrease with increasing q where

$$q = |\underline{k} - \underline{k}'| \ . \tag{51}$$

Evenson and Liu (1968b) have shown that for the heavy rare-earth metals the observed magnon spectra can be accurately reproduced by assuming that the matrix elements have a gaussian dependence on q. There is no such data available for the lighter rare-earths so it is assumed here that a similar approximation can be utilized. These matrix elements can be written as

$$J^2(q) = J^2(0)e^{-(q/q_o)^2} \tag{52}$$

where q_o is chosen to correspond to the size of the 4f shell.

B. Results of the Calculations

The generalized susceptibilities were first calculated using a constant value for the matrix element J(q). The results of these calculations are presented in Figures 20 and 21. The lines shown in these drawings are contours of constant χ and the values given are in states per Rydberg per atom. The peaks in the curve correspond to those nestings between Fermi surface regions described in the preceding chapter. The principal peaks near the origin are due to the nesting between portions of seventh zone electron surface shown by $\underline{q}_1$, $\underline{q}_2$ and $\underline{q}_3$ in Figure 19. The maximum value of χ in this region is near $q_x = .125b_1$ and $q_z = .08b_3$.

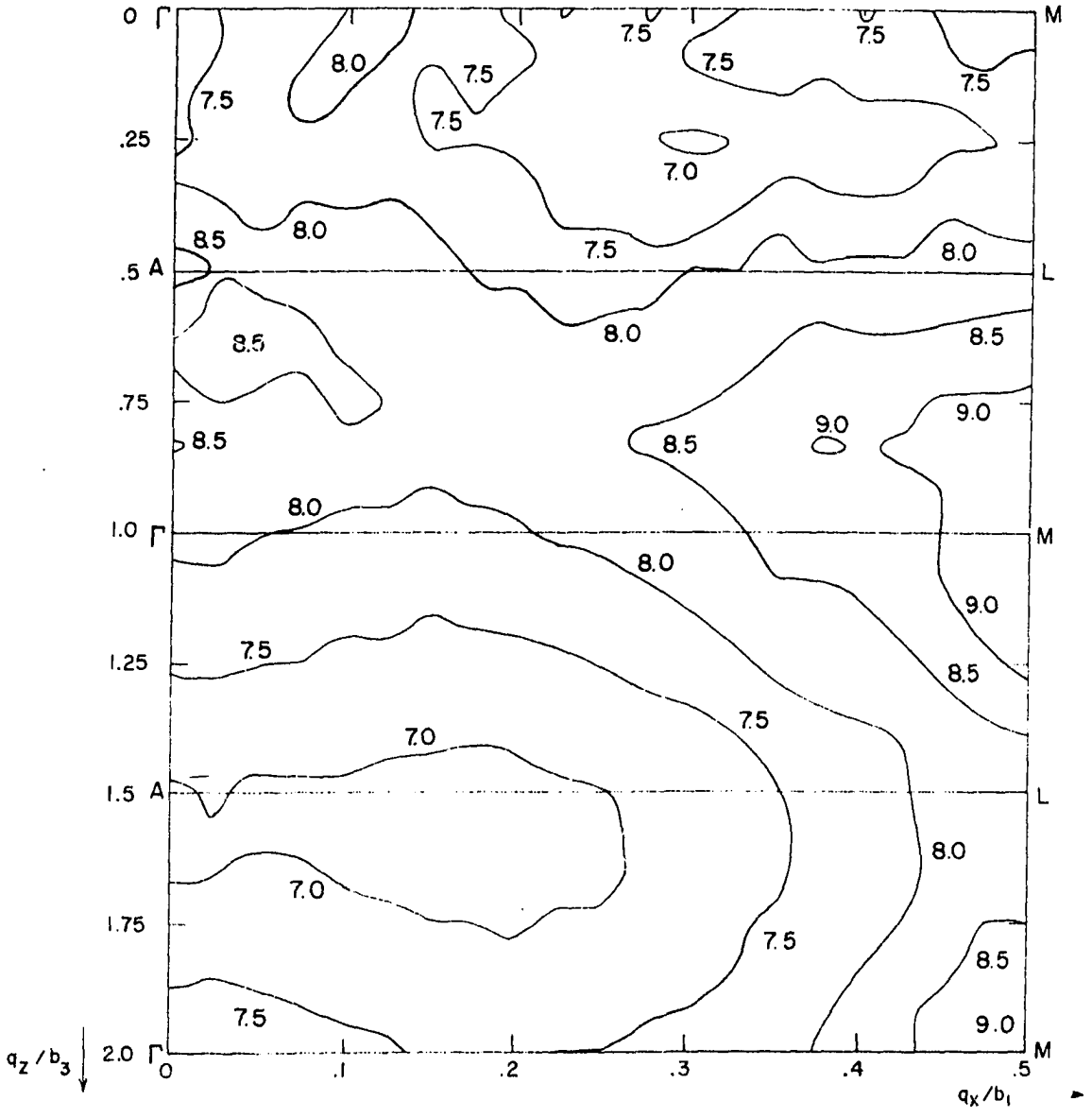

Figure 20. Contours (states/ryd/atom) of equal susceptibility for praseodymium assuming a constant exchange matrix element

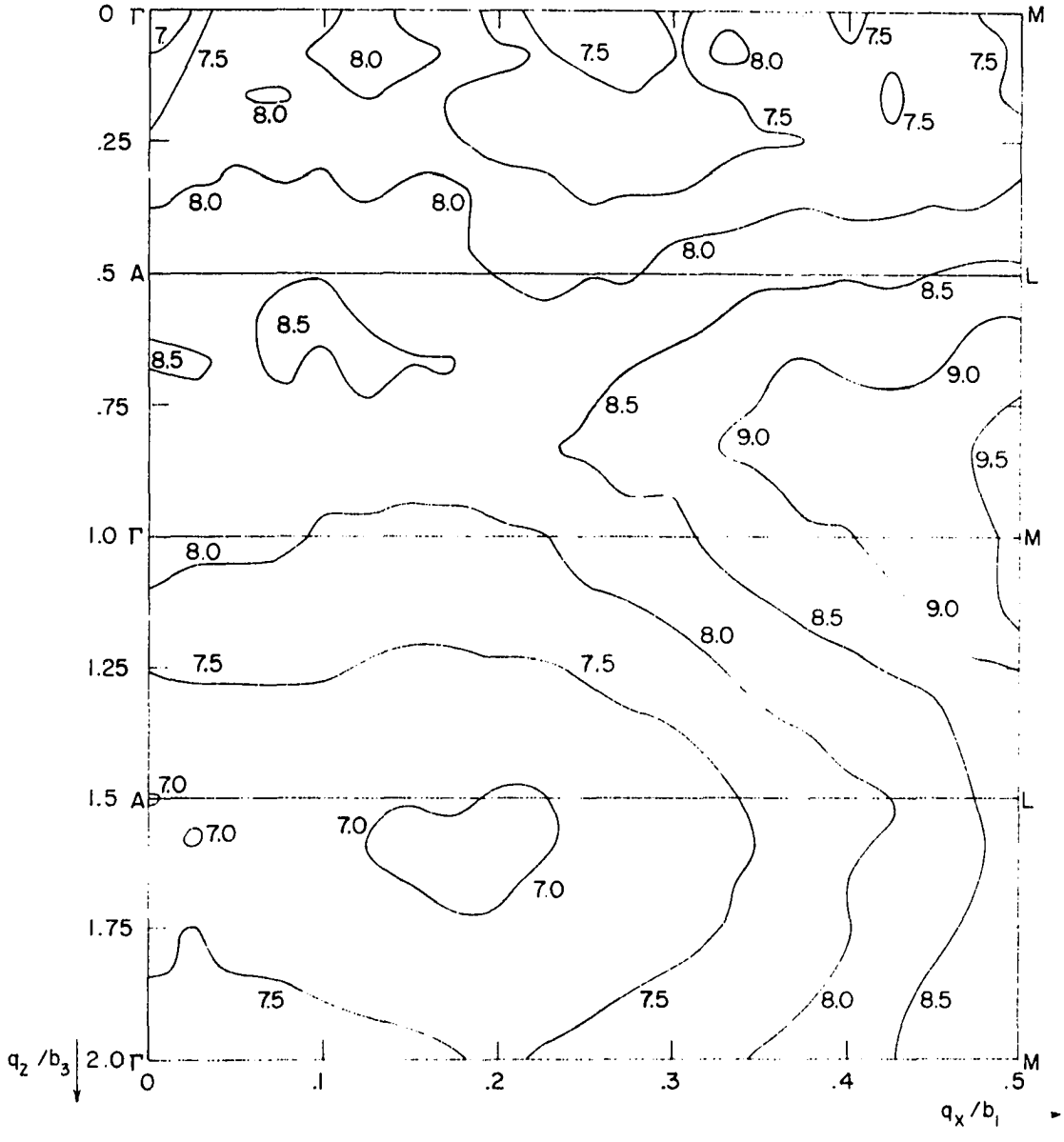

Figure 21. Contours (states/ryd/atom) of equal susceptibility for neodymium assuming a constant exchange matrix element

A large peak occurs in the second branch of the susceptibility curve for small q_x. This is located near $q_z = .65b_3$ and is centered at $q_x = .04b_1$ for Pr and at $q_x = .12b_1$ for Nd. This peak is due to a nesting between seventh and eighth zone electron surfaces separated by a wave vector approximately equal to the vector $\underline{q}_1$ shown in Figure 19.

The nesting of fifth and sixth zone surfaces into themselves and each other across the center (ΓA) of the zone produces the large values of χ near $q_x = .4b_1$ and for $q_z = .25b_3$ and $.75b_3$. These peaks are masked somewhat by the general rise of the $\chi(q)$ curve near the point M in branches 2 and 3. This rise is not due to any feature of the Fermi surface but occur because this wave vector separates large regions of occupied k-space from large unoccupied regions. In this case χ becomes large not because of a small energy denominator in Equation 50 but due to a great number of terms for which $f_{\underline{k}} = 1$ and $f_{\underline{k}+\underline{q}} = 0$.

The generalized susceptibilities were next calculated using gaussian matrix elements as given in Equation 52. If the width of the 4f shell is approximately one-tenth of the nearest neighbor distance in the crystal then

$$q_o \simeq 2.5b_3 \tag{53}$$

In order to see how critical the choice of q_o would be, generalized susceptibilities were calculated for both metals with (a) $q_o = 2b_3$ and (b) $q_o = 3b_3$.

The first results which correspond to a less localized 4f shell are shown in Figures 22 and 23 and the other sets of values are shown in Figures 24 and 25. In both cases there is a large peak near $q_x = .125b$ and $q_z = 0$ for both metals. For the case where $q_o = 3b_3$ there is also a peak near the

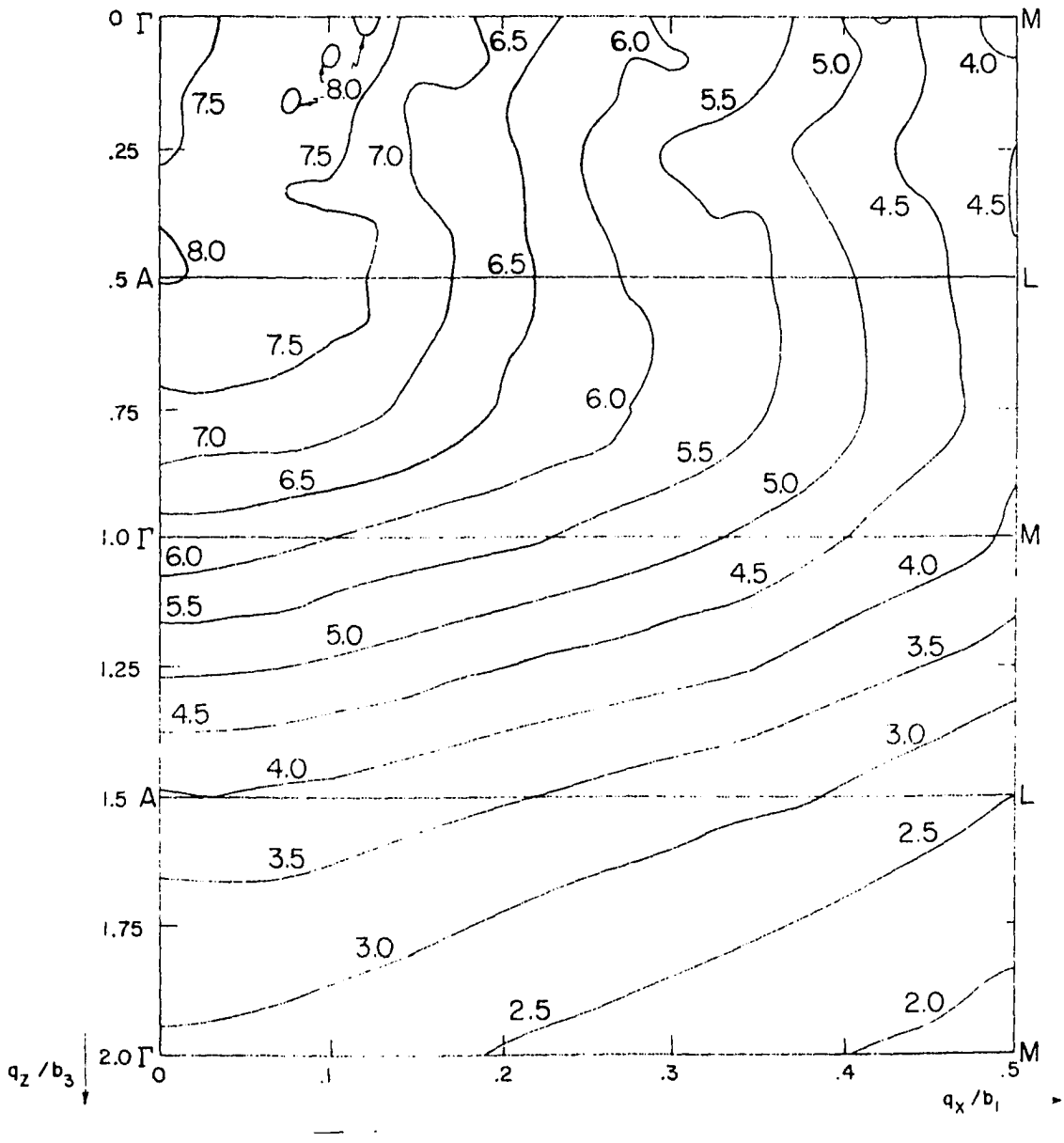

Figure 22. Contours (states/ryd/atom) of equal susceptibility for praseodymium. A gaussian matrix element with $q_o = 2b_3$ is assumed

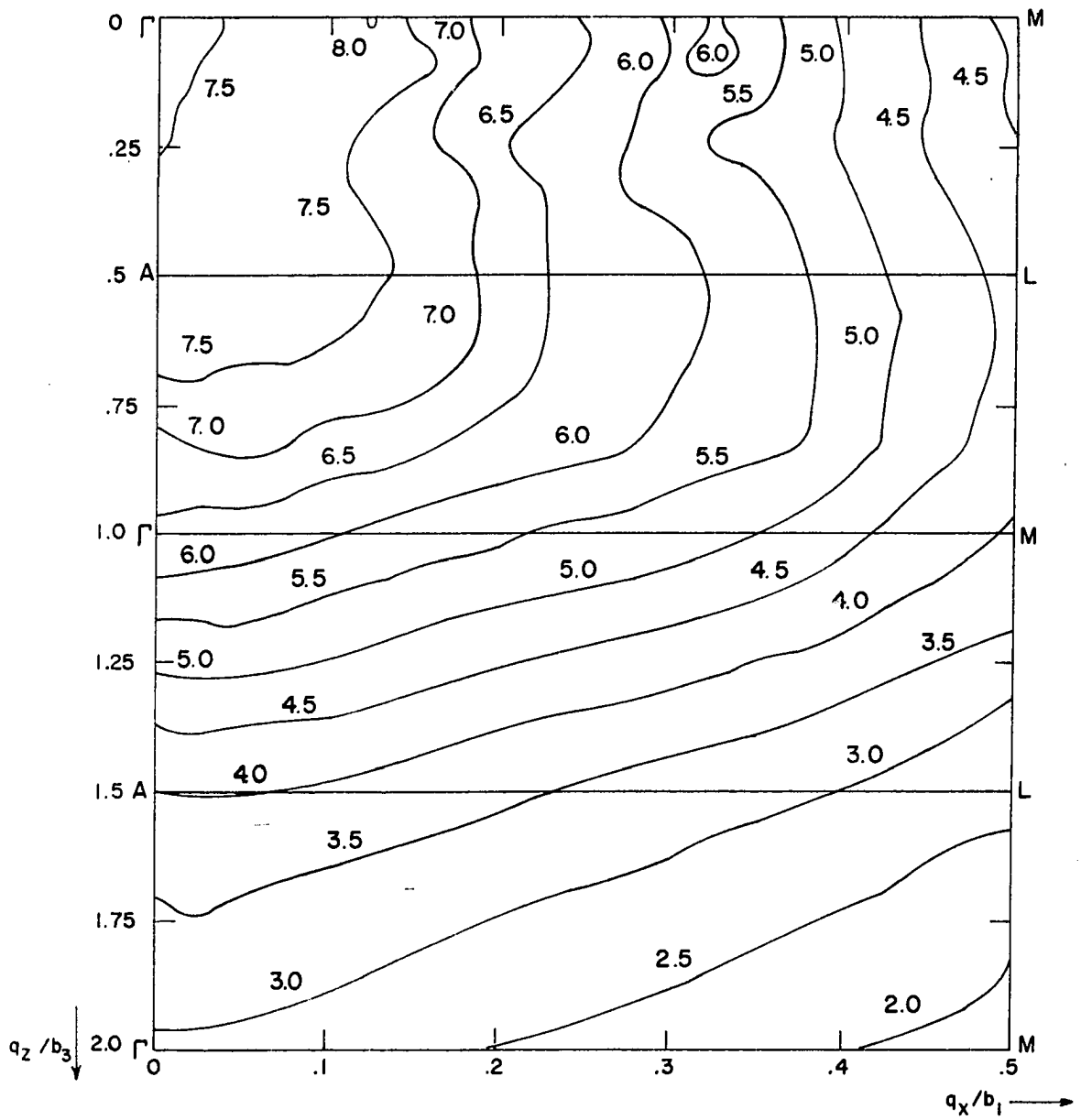

Figure 23. Contours (states/ryd/atom) of equal susceptibility for neodymium. A gaussian matrix element with $q_o = 2b_3$ is assumed

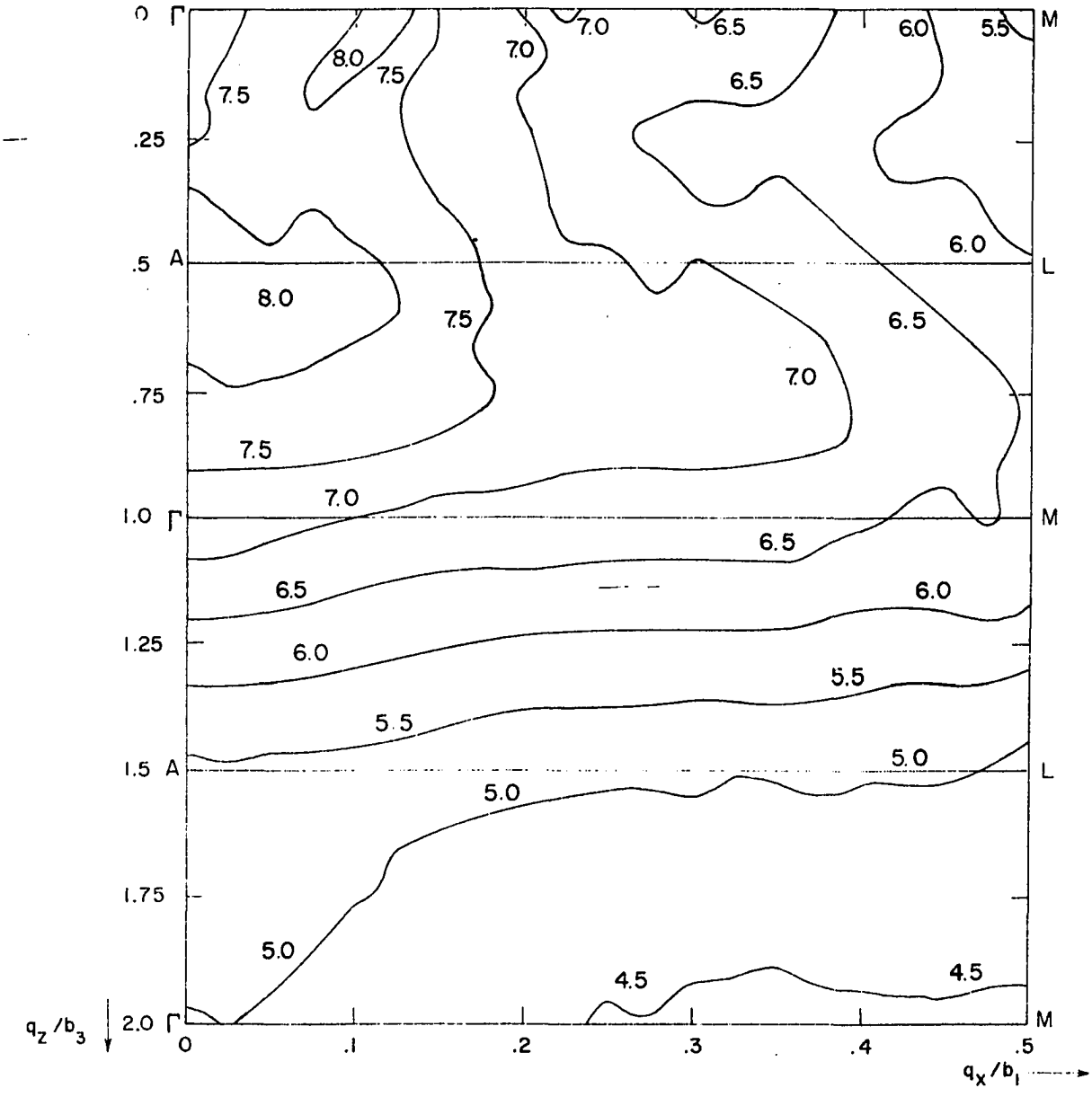

Figure 24. Contours (states/ryd/atom) of equal susceptibility for praseodymium. A gaussian matrix element with $q_o = 3b_3$ is assumed

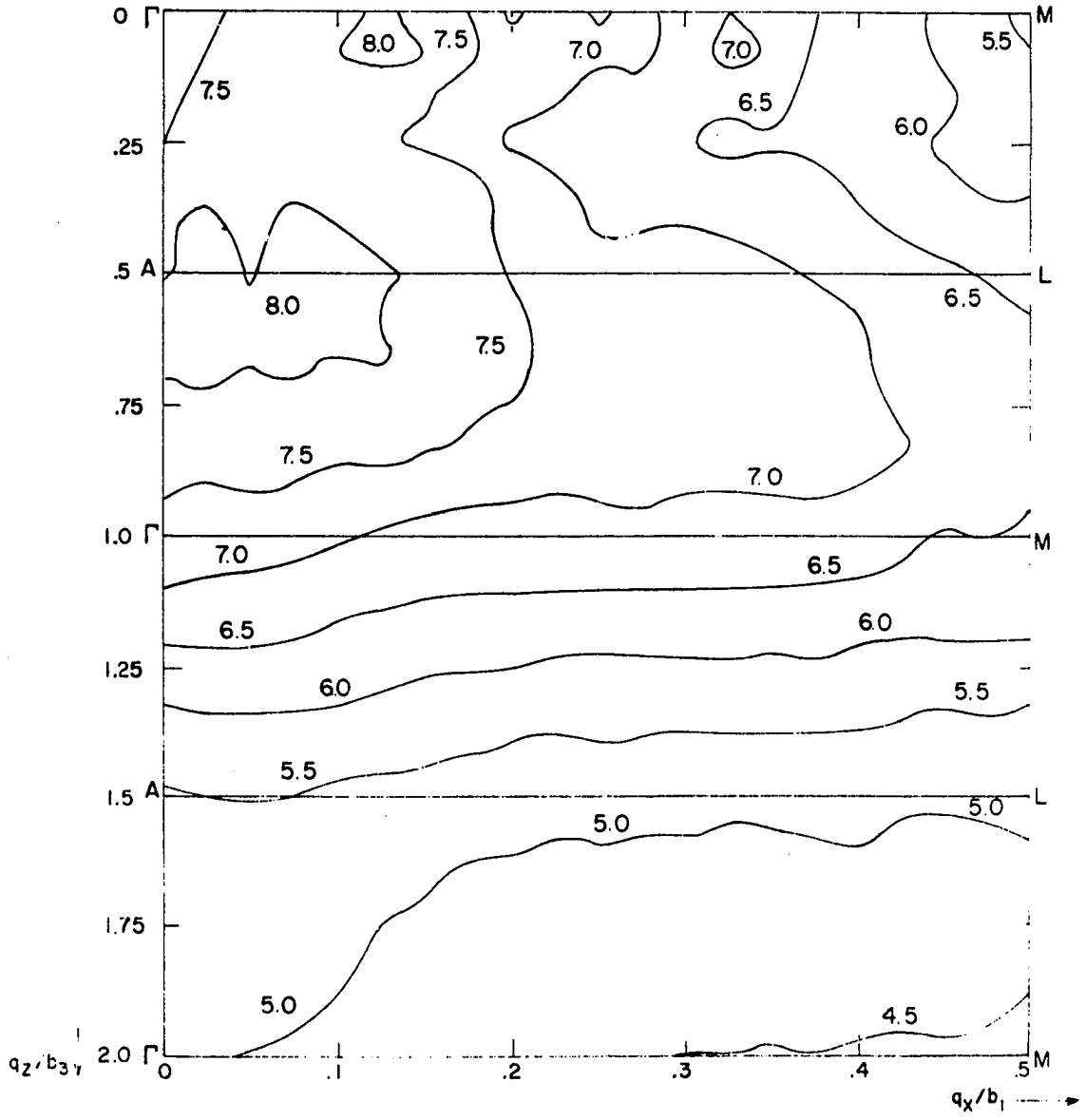

Figure 25. Contours (states/ryd/atom) of equal susceptibility for neodymium. A gaussian matrix element with $q_o = 3b_3$ is assumed

point A in the first branch of the $\chi(q)$ curve. This peak is present for both metals but is more prominent in Pr. For the less localized interaction this maxima becomes quite broad extending out to a value of q_x of $.125b_1$. In the case of Pr the peak value of χ in this region still occurs at the point A but for Nd the maximum is located at $q_x = .075b_1$ and $q_z = .58b_3$.

A check on the accuracy of the susceptibility calculations can be made by comparing these results with the density of states calculations presented previously. It has been shown (Evenson 1968) that

$$\chi(0) = \frac{1}{2}N(E_F) \tag{54}$$

where $N(E_F)$ is the density of states at the Fermi energy. Because of the finite mesh used the value of $\chi(0)$ computed is zero but a reasonable value of $\chi(0)$ can be obtained by extrapolating the calculated $\chi(q)$ curve to $q = 0$. These results are compared in Table 5. Although the values differ by about 20 percent, the possible error in the value $N(E_F)$ used is about this same size as can be seen from the density of states curves presented in a previous section. Thus the agreement between $\chi(0)$ and the density of states at the Fermi energy is as good as can be expected.

Table 5. Density of states at the Fermi energy, $N(E_F)$, and generalized susceptibility for zero wave vector, $\chi(0)$, for Pr and Nd

Metal	$1/2N(E_F)$ (states/Ryd/atom)	$\chi(0)$
Pr	8.1	6.8
Nd	8.4	6.9

VII SUMMARY AND CONCLUSIONS

This investigation has been concerned with the electronic band structure of the double hexagonal close-packed structure of lanthanum praseodymium and neodymium and the relationship of the bands to physical properties of the metals.

The calculated values of the density of states at the Fermi energy for the three metals are about 20 to 30 percent below the values necessary to produce the electronic specific heats which have been experimentally observed. This indicates that the specific heat is enhanced by the electron-phonon interaction. For La the experimental and calculated results differ by an amount approximately equal to that predicted by McMillan (1968).

The Fermi surfaces differ from those of the hexagonal close-packed heavy rare-earths in two major respects. The most noticeable feature is the absence of the large flat regions perpendicular to the c-axis. This appears to result from the potential in the dhcp lattice which differs slightly from the potential of the hcp lattice. In hcp metals there are flat pieces of Fermi surface near the center of the Brillouin zone. The dhcp potential has the additional periodicity required to lower the energy of states in this region by eliminating these pieces of Fermi surface.

The difference in magnetic ordering between the light and heavy rare-earths may be understood from the difference in their Fermi surfaces. In the heavier metals the nesting of states near one of the flat pieces into states near another produces the maximum in the generalized susceptibility. Evenson and Liu (1968a) showed the connection between this maximum and the periodicity of the ordered magnetic structures.

With the elimination of these regions the principal nesting in the light rare-earths occurs between portions of Fermi surface which are essentially perpendicular to the b-axis. Thus the principal magnetic periodicity of the light rare-earths will be in the basal plane rather than along the c-axis.

The periodicity of this ordering is derived from the generalized susceptibility of the metal. These generalized susceptibilities were calculated for Nd and Pr using an exchange matrix element which had a gaussian dependence on the wave vector q. The range of the gaussian was chosen to be consistent with the dimension of the region in which the 4f and conduction electrons interact. These calculations indicate that the wave vector of the magnetic ordering periodicity lies in one of the b directions and has a magnitude of $.125b_1$. This result is in very close agreement with the experimental value of $.13b_1$ determined from neutron diffraction measurements by Moon, et al., (1964) for Nd and by Cable, et al., (1964) for Pr.

There are two features of the magnetic structure model given by Koehler (1965) which cannot be predicted from the susceptibility curves. The most noticeable difference is that there is no periodicity along the c-axis indicated from our calculation whereas Koehler's model shows the moments in alternate layers having hcp nearest neighbors being ordered antiferromagnetically. While it may be possible that a model could be constructed which would be consistent with both the experimental data and the results presented here, it is more likely that there is some additional interaction which must be included to completely explain the magnetic structure.

A less prominent peak is found in the susceptibility curve correspond-

ing to a wave vector which would give the correct c-axis periodicity. However, the component of this wave vector in the basal plane is much smaller than the experimentally determined value.

The other experimental result which is not indicated by the susceptibility results is the second ordering which is observed in Nd but not in Pr. There are no major differences in the susceptibilities of the two metals which could be related to a second ordering. This leads one to the belief that the two sublattices in the dhcp crystal are not weakly coupled. If this is indeed true the paramagnetic bands cannot be expected to predict this additional ordering.

VIII REFERENCES

Anderson, O. K. and Loucks, T. L. 1968. Phys. Rev. 167, 551.

Cable, J. W., Moon, R. M., Koehler, W. C. and Wollen, E. O. 1964. Phys. Rev. Letters 12, 553.

Callaway, J. 1964. Energy Band Theory. New York, Academic Press, Inc.

Dimmock, J. O. and Freeman, A. J. 1964. Phys. Rev. Letters 13, 750.

Elliott, R. J. 1965. Theory of magnetism in the rare earth metals. In Rado, G. T. and Suhl, H., eds. Magnetism. Vol. 2. Part A. Pp. 385-424 New York, Academic Press, Inc.

Evenson, W. E. 1968. Generalized susceptibilities and magnetic ordering of heavy rare earths. Unpublished Ph.D. thesis. Ames, Iowa, Library, Iowa State University of Science and Technology.

Evenson, W. E. and Liu, S. H. 1968a. Phys. Rev. Letters, 21, 432.

Evenson, W. E. and Liu, S. H. 1968b. Phys. Rev., to be published.

Falicov, L. M. and Cohen, M. H. 1962. Phys. Rev. 130, 92.

Freeman, A. J., Dimmock, J. O. and Watson, R. E. 1966. Phys. Rev. Letters 16, 94.

Gschneidner, K. A. 1965. An experimental approach to simplified band structure of the rare-earth metals. In Eyring, L., ed. Rare Earth Research III. New York, Gordon and Breach.

Gschneidner, K. A. 1961. Rare Earth Alloys. Princeton, D. Van Nostrand Co., Inc.

Herman, F. and Skillman, S. 1963. Atomic Structure Calculations. Englewood Cliffs, N. J., Prentice-Hall, Inc.

Herring, C. 1966. Exchange interactions among itinerant electrons. In Rado, G. T. and Suhl, H., eds. Magnetism. Vol. 4. New York, Academic Press, Inc.

Johnson, D. L. and Finnemore, D. K. 1967. Phys. Rev. 158, 376.

Kasuya, T. 1956. Progr. Theo. Phys. (Kyoto) 16, 45.

Kasuya, T. 1966. S-d and s-f interaction and rare-earth metals. In Rado, G. T. and Suhl, H. Magnetism. Vol. 2. Part B. Pp. 215-294 New York, Academic Press, Inc.

Keeton, S. C. 1966. Relativistic energy bands and Fermi surfaces for some heavy elements. Unpublished Ph.D. thesis. Ames, Iowa, Library, Iowa State

University of Science and Technology.

Keeton, S. C. and Loucks, T. L. 1968. Phys. Rev. 168, 672.

Koehler, W. C. 1965. J. Appl. Phys. 36, 1078.

Liberman, D., Waber, J. T. and Cromer, D. T. 1965. Phys. Rev. 137, A27.

Liu, S. H. 1961. Phys. Rev. 121, 451.

Lomer, W. M. 1962. Proc. Phys. Soc. 80, 489.

Loucks, T. L. 1965. Phys. Rev. 139, 231.

Loucks, T. L. 1967. Augmented Plane Wave Method. New York, W. A. Benjamin, Inc.

Lowdin, P. O. 1956. Advan. Phys. 5, 1.

Mattheiss, L. F. 1964. Phys. Rev. 133, A1399.

Mattis, D. C. 1965. The Theory of Magnetism. New York, Harper and Row, Inc.

Mattis, D. C. and Donath, W. E. 1962. Phys. Rev. 128, 1618.

McMillan, W. L. 1968. Phys. Rev. 167, 331.

Moon, R. M., Cable, J. W. and Koehler, W. C. 1964. J. Appl. Phys. Suppl. 35, 1041.

Nagamiya, T. 1967. Theory of helical spin configurations. In Seitz, F., Turnbull, D., and Ehrenreich, H., eds. Solid State Physics. Vol. 20. Pp. 306-411 New York, Academic Press, Inc.

Overhauser, A. W. 1963. J. Appl. Phys. 34, 1019.

Pearson, W. B. 1958. Handbook of Lattice Spacings and Structures for Metals. New York, Pergamon Press.

Pennington, R. H. 1965. Introductory Computer Methods and Numerical Analysis. New York, The Macmillan Co.

Roth, L. M., Zieger, H. J. and Kaplan, T. A. 1966. Phys. Rev. 149, 519.

Ruderman, M. A. and Kittel, C. 1954. Phys. Rev. 96, 99.

Slater, J. C. 1937. Phys. Rev. 51, 846.

Slater, J. C. 1951. Phys. Rev. 81, 385.

Villain, J. 1959. J. Phys. Chem. Solids 11, 303.

Waber, J. T. and Switendick, A. C. 1965. Unpublished multilithed paper presented at Fifth Rare Earth Research Conference, Ames, Iowa. Evanston, Illinois, Northwestern University, Department of Materials Science.

Watson, R. C., Freeman, A. J. and Dimmock, J. O. 1968. Phys. Rev. 167, 497.

Yosida, K. 1957. Phys. Rev. 106, 893.

Ziman, J. M. 1965. Principles of the Theory of Solids. London, England, Cambridge University Press.

IX ACKNOWLEDGEMENTS

The author would like to acknowledge his gratitude to Professor S. H. Liu for his active guidance and encouragement in this investigation. A deep indebtedness is also owed to Dr. T. L. Loucks who suggested the project and provided its early direction. His continued interest in this project has been of great value and is duely appreciated.

The author would also like to thank Dr. W. E. Evenson for many enlightening discussions relating to this work. He is also appreciative of the cooperation received from the Ames Laboratory Computer Services Group and would like to thank the Ames Laboratory for their financial support during the course of this study.